MONTANA STATE UNIVERSITY LIBRARY

# Extensive remodeling of the photosynthetic apparatus alters energy transfer among photosynthetic complexes when cyanobacteria acclimate to far-red light

Authors: Ming-Yang Ho, Dariusz M. Niedzwiedzki, Craig MacGregor-Chatwin, Gary Gerstenecker, C. Neil Hunter, Robert E. Blankenship, and Donald A. Bryant

© 2020. This manuscript version is made available under the CC-BY-NC-ND 4.0 license https://creativecommons.org/licenses/by-nc-nd/4.0/

Ho, Ming-Yang, Niedzwiedzki, Dariusz M., MacGregor-Chatwin, Craig, Gerstenecker, Gary, Hunter, C. Neil, Blankenship, Robert E., & Bryant, Donald A. (2019). Extensive remodeling of the photosynthetic apparatus alters energy transfer among photosynthetic complexes when cyanobacteria acclimate to far-red light (Version Accepted Version). Biochimica Et Biophysica Acta (BBA) - Bioenergetics, 1861(4), 148064. http://doi.org/10.1016/j.bbabio.2019.148064

Made available through Montana State University's ScholarWorks
scholarworks.montana.edu

# Extensive remodeling of the photosynthetic apparatus alters energy transfer among photosynthetic complexes when cyanobacteria acclimate to far-red light

**Ming-Yang Ho[a,b,1], Dariusz M. Niedzwiedzki[c], Craig MacGregor-Chatwin[d], Gary Gerstenecker[c], C. Neil Hunter[d], Robert E. Blankenship[c,e], and Donald A. Bryant[a,b,f,*]**

[a]*Department of Biochemistry and Molecular Biology, The Pennsylvania State University, University Park, PA USA*

[b]*Intercollege Graduate Program in Plant Biology, The Pennsylvania State University, University Park, PA USA*

[c]*Department of Energy, Environmental & Chemical Engineering and Center for Solar Energy and Energy Storage, Washington University, St. Louis, MO USA*

[d]*Department of Molecular Biology and Biotechnology, University of Sheffield, Sheffield UK*

[e]*Departments of Biology and Chemistry, Washington University, St. Louis, MO USA*

[f]*Department of Chemistry and Biochemistry, Montana State University, Bozeman, MT USA*

[1]Present address: Plant Research Laboratory, Michigan State University, MI USA

***Address for Correspondence:** Dr. Donald A. Bryant, S-002 Frear Laboratory, Department of Biochemistry and Molecular Biology, The Pennsylvania State University, University Park, PA 16802 USA. Phone; 814-865-1992; Fax: 814-863-7024; E-mail: dab14@psu.edu

**ABSTRACT**

Some cyanobacteria remodel their photosynthetic apparatus by a process known as Far-Red Light Photoacclimation (FaRLiP). Specific subunits of the phycobilisome (PBS), photosystem I (PSI), and photosystem II (PSII) complexes produced in visible light are replaced by paralogous subunits encoded within a conserved FaRLiP gene cluster when cells are grown in far-red light (FRL; λ = 700-800 nm). FRL-PSII complexes from the FaRLiP cyanobacterium, *Synechococcus* sp. PCC 7335, were purified and showed to contain Chl *a*, Chl *d*, Chl *f*, and pheophytin *a*, while FRL-PSI complexes contained only Chl *a* and Chl *f*. The spectroscopic properties of purified photosynthetic complexes from *Synechococcus* sp. PCC 7335 were determined individually, and energy transfer kinetics among PBS, PSII, and PSI were analyzed by time-resolved fluorescence (TRF) spectroscopy. Direct energy transfer from PSII to PSI was observed in cells (and thylakoids) grown in red light (RL), and possible routes of energy transfer in both RL- and FRL-grown cells were inferred. Three structural arrangements for RL-PSI were observed by atomic force microscopy of thylakoid membranes, but only arrays of trimeric FRL-PSI were observed in thylakoids from FRL-grown cells. Cells grown in FRL synthesized the FRL-specific complexes but also continued to synthesize some PBS and PSII complexes identical to those produced in RL. Although the light-harvesting efficiency of photosynthetic complexes produced in FRL might be lower in white light than the complexes produced in cells acclimated to white light, the FRL-complexes provide cells with the flexibility to utilize both visible and FRL to support oxygenic photosynthesis.

**Keywords:** photosynthesis; phycobilisome; photosystem I; photosystem II; far-red light photoacclimation

**Abbreviations used:** AFM, atomic force microscopy; AP, allophycocyanin; Chl, chlorophyll; EAS, evolution-associated spectra; EAFS, evolution-associated fluorescence spectra; FaRLiP, far-red light photoacclimation; FRL, far-red light; HPLC, high performance liquid chromatography; IMAC, immobilized metal-affinity chromatography; LC-MS/MS, liquid chromatography and tandem mass spectroscopy; PBP, phycobiliprotein(s); PBS, phycobilisome(s); PC, phycocyanin; PCR, polymerase chain reaction; PE, phycoerythrin; PSI, photosystem I; PSII, photosystem II; RP-HPLC, reversed-phase HPLC; SVD, singular-value decomposition; TRF, time-resolved fluorescence.

## 1.0 Introduction

Most cyanobacteria are chlorophyll (Chl) *a*-dependent photoautotrophs that use visible light to perform oxygenic photosynthesis [1]. The light energy used by these chlorophototrophs is absorbed and transduced by three supramolecular, pigment-binding protein complexes: photosystems I and II (PSI and PSII) and the phycobilisome (PBS) [2]. The X-ray crystal structures of cyanobacterial PSI and PSII are known, and these structures show that these proteins employ 96 and 35 chlorophyll (Chl) *a* molecules, and 22 and 11 carotenoids (predominantly β-carotene), respectively, for light harvesting [3, 4]. Because Chl *a* molecules absorb mainly blue and red light, PBS are used by cyanobacteria and red algae to harvest visible light in the wavelength range 500 to 650 nm (green to orange light) [2]. PBS are supramolecular (~5-20 MDa) antenna protein complexes that are mostly composed of brilliantly colored, water-soluble proteins, phycobiliproteins (PBP), which carry one or more covalently attached, linear tetrapyrrole chromophores [5]. A complete structural model is available for the hemidiscoidal PBS of *Nostoc* sp. PCC 7120 [6]. In this type of PBS, peripheral rods are formed from linker proteins and phycocyanin (PC; $\lambda_{max}$ = 620 nm), and variably phycoerythrin (PE; $\lambda_{max}$ = 560 nm) or phycoerythrocyanin (PEC; $\lambda_{max}$ = 575 nm) [2, 5, 7]. The core cylinders of hemidiscoidal PBS are mostly formed from allophycocyanin (AP; $\lambda_{max}$ = 650 nm) [8], but these also include two so-called terminal emitters, allophycocyanin-B (ApcD; $\lambda_{max}$ = 670 nm) and a core-membrane linker PBP, ApcE ($\lambda_{max}$ = ~670 nm). ApcE and ApcD mediate energy transfer from PBS to PSII and PSI, respectively [2, 9-11].

Cyanobacteria are not the only phototrophs that primarily use visible light as energy source. Plants, algae, and other chlorophototrophic bacteria are all potential competitors for visible light. Because of the intense competition for light, some terrestrial cyanobacteria have evolved a specific mechanism to enhance light harvesting in environments enriched in far-red light (FRL, λ = 700 to 800 nm). This mechanism, known as **Fa**r-**R**ed **Li**ght **P**hotoacclimation (FaRLiP), occurs in terrestrial cyanobacteria that inhabit light niches where FRL predominates due to physical properties of light (e.g., wavelength-dependent light

scattering or strong filtering of light by absorption by Chl *a* and/or Chl *b*). Examples of such environments include the shade of plants, tropical soil ecosystems, soil crusts, microbial mats, dense algal blooms, beach rocks, and stromatolites [12-20]. Chl *d* and Chl *f* are synthesized during FaRLiP, and PSI, PSII, and PBS are extensively remodeled to facilitate the absorption of FRL for growth [14, 21-23]. FaRLiP cyanobacteria, including *Synechococcus* sp. PCC 7335 (hereafter *Synechococcus* 7335) investigated here, contain a conserved cluster of 20 genes [14, 22]. This gene cluster encodes Chl *f* synthase (ChlF), a photosensor (RfpA) and response regulators (RfpB and RfpC) to activate the expression of the twenty genes in the FaRLiP cluster, and genes encoding paralogous subunits to remodel the PBS core, PSII, and PSI and thereby allow growth in FRL [14, 22-29].

Previous studies have described some of the properties of the modified PBS that are produced in cyanobacteria grown in FRL (14, 26, 27, 30). However, unlike far more comprehensive studies of PBP and PBS from cells grown in white-light (WL) and that do not absorb FRL [2, 11, 31-33], the pathway and kinetics of energy transfer in FRL-absorbing bicylindrical cores (hereafter FRL-BC) are still unresolved issues. FRL-PSI complexes containing Chl *f* have been isolated and characterized from five strains: *Leptolyngbya* sp. JSC-1, *Chroococcidiopsis thermalis* PCC 7203, *H. hongdechloris*, *Fischerella thermalis* PCC 7521, and *Synechococcus* 7335 [14, 28, 29, 34, 35]. The FRL-PSI complexes from all five strains have red-shifted fluorescence emission due to the presence of Chl *f* in the complexes; however, the maximal fluorescence emission wavelength at 77 K varies from about 738 to 750 nm for the various complexes studied to date. Only the FRL-PSII complexes of *Chroococcidiopsis thermalis* PCC 7203 have been described in detail, and it is thus uncertain how general conclusions about FRL-PSII might be [34]. Furthermore, no comprehensive studies of all photosynthetic complexes from a single FaRLiP cyanobacterium have been conducted in order to evaluate critically the energy transfer processes occurring in cells acclimated to FRL.

In this study we purified FRL-PSII from *Synechococcus* 7335, and together with previous studies of PSI and PBP complexes from this strain, the pigment compositions and absorption and fluorescence

emission properties for the three major complexes in the photosynthetic apparatus derived from cells grown in visible light (WL or RL) and FRL are now known [27, 29, 36, this study]. Atomic force microscopy was employed to monitor changes in the organization of PSI and PSII complexes in thylakoids from cells grown in RL or FRL. Time-resolved fluorescence (TRF) spectroscopy was used to deconvolute the previously unidentified emission features arising from PSII and FRL-AP at low-temperature and their kinetics [27]. In addition to these spectroscopic studies, tryptic peptide fingerprinting by LC-MS/MS was employed to provide information concerning the subunit composition of the photosynthetic complexes produced in FRL. By first determining the absorption and fluorescence emission characteristics at low-temperature for the major photosynthetic complexes produced in RL and FRL, we infer the pathways of excitation energy transfer in isolated complexes, thylakoids, and whole cells of *Synechococcus* 7335.

## 2.0 Materials & methods

### *2.1 Strains and growth conditions*

*Synechococcus* sp. PCC 7335 was obtained from the Pasteur Culture Collection (https://www.pasteur.fr/en/pcc) [37]. The growth medium (ASN-III), growth conditions, and light conditions were the same as previously described [25, 27, 37, 38]. Cells were cultured at room temperature (~25°C). White light (WL) was provided by cool white fluorescent bulbs at irradiances ranging from 25 to 200 μmol photons $m^{-2}$ $s^{-1}$ as indicated. Red light (RL) or green light (GL) was provided at ~25 μmol photons $m^{-2}$ $s^{-1}$ by filtering the fluorescent light with red or green plastic filters [14, 27, 39]. An LED panel with emission centered at 720 nm and halogen light filtered by a combination of green and red plastic filters were used to provide far-red light at ~180 μmol photons $m^{-2}$ $s^{-1}$ [14, 39]. Growth of cells was monitored as optical density at 750 nm by using a GENESYS 10 spectrophotometer (ThermoSpectronic, Rochester, NY).

### *2.2 Generation of a strain expressing His-tagged PsbC2*

To generate a strain producing a $[His]_6$-tagged variant of PsbC2, a plasmid to insert a $[His]_6$-tag and a kanamycin resistance cassette (*aphAII*) was designed and transferred to *Synechococcus* 7335 by

conjugation. A scheme showing the design of the construct appears in **Fig. S1A**, and the primers used for polymerase chain reaction (PCR) are listed in **Table S1**. Sequences encoding a $[His]_6$-tag and the *aphAII* cassette were designed to be inserted at the 3´end of *psbC2*. A similar strategy was successfully used to purify oxygen-evolving PSII from *Thermosynechococcus elongatus* [40]. Methods for generating the construct and for conjugal transfer of the plasmid to cyanobacteria were described in previous publications [24, 25, 38, 41]. A fragment extending 3-kbp upstream from the stop codon of *psbC2* was amplified by primers P1 and P2, and another 3-kbp fragment extending downstream from *psbC2* was amplified by primers P5 and P6 (**Fig. S1A**). Primers P3 and P4 were used to amplify the $[His]_6$-tag and the *aphIIA* gene. The three PCR amplicons were digested by the appropriate restriction enzymes, ligated together, and amplified by PCR. The entire ~7-kb fragment was then cloned into the cargo plasmid, pRL277 [42]. The sequence of the inserted fragment was confirmed by DNA sequencing. Conjugal transfer of the resulting plasmid from *Escherichia coli* to *Synechococcus* 7335 was performed as previously described [25, 38]. Transconjugant colonies were selected and streaked on ASN-III plates supplemented with kanamycin (100 μg $ml^{-1}$). Colony PCR (primers P7 and P8) and DNA sequencing were performed to confirm the insertion of $[His]_6$-tag and the kanamycin resistance cassette in the genome (**Fig. S1B**).

### *2.3 Purification of PSII complexes*

The preparation of thylakoid membranes was performed as described by [14] with minor modifications. *Synechococcus* 7335 cells expressing $[His]_6$-tagged PsbC2 that had been grown in FRL were harvested and resuspended in thylakoid isolation buffer (50 mM MES, pH 6.5, 10 mM $CaCl_2$, and 10 mM $MgCl_2$). Resuspended cells were broken by three passages through a French pressure cell at 138 MPa at 4 °C as previously described [27]. After centrifugation at 3,830 × *g* to remove unbroken cells and large cell debris, thylakoid membranes were pelleted by ultracentrifugation at 126,100 × *g* at 4 °C for 30 min. The thylakoid membranes were resuspended in thylakoid isolation buffer, the Chl concentration was adjusted to 0.4 mg Chl $ml^{-1}$, *n*-dodecyl-β-D-maltoside (DM) was added to a final concentration of 1% (w/v), and the solution was incubated at 4 °C for 1 hour. PSII was purified as previously described with minor

modifications [41]. Ni-NTA resin ($Ni^{+2}$ ion chelated by nitrilotriacetic acid; G-Biosciences, St. Louis, MO) was used to bind the His-tagged PSII complexes, and PSII complexes were precipitated by adding PEG-3350 to a final concentration of 12.5% (w/v) from a stock 25% stock solution prepared with thylakoid isolation buffer.

### *2.4 Pigment extraction and analysis*

Samples (thylakoid membranes or PSII complexes) containing roughly equivalent amounts of Chl in 10 µl of thylakoid isolation buffer were mixed with iodoacetamide (10 µl of a 36 mg $ml^{-1}$ stock solution) and with 180 µl of acetone:methanol (7:2). The mixture was vortexed and incubated on ice for 10 min to extract pigments. After centrifugation at 15,294 × *g* for 3 min, the resulting supernatant was filtered and analyzed by reversed-phase high performance liquid chromatography (RP-HPLC) as previously described. The methods for the RP-HPLC analysis and calculations to determine pigment concentrations and the percentage content for each pigment were performed as previously described [28, 42].

### *2.5 Trypsin digestion and proteomics analysis*

The digestion of proteins with trypsin and subsequent LC-MS/MS analyses were performed at the mass spectroscopy core facility of the Photosynthetic Antenna Research Center (PARC) at Washington University in St. Louis. The methods for sample preparation and analysis have been described [25, 28]. The resulting mass data were analyzed by Mascot v. 2.6 using databases comprising the FASTA files specific for *Synechococcus* 7335 and included common contaminants (cRAP database) using a reverse decoy approach to reduce false positives. The same databases and reverse decoys were also analyzed using the Sequest algorithm within Protein Discoverer v. 2.2. The results were combined in Scaffold v. 4.85 and were also searched using the X-Tandem algorithm to assist in the elimination of false positives.

### *2.6 Steady-state absorption and low-temperature (77 K) fluorescence spectroscopy*

Aliquots of whole cells were resuspended in ASN-III medium and adjusted to $OD_{750}\,ml^{-1} = 0.25$ for absorption and $OD_{750}\,ml^{-1} = 0.5$ for fluorescence measurements. Thylakoid membranes and purified PSI and PSII complexes were diluted in thylakoid isolation buffer supplemented with 0.01 % (w/v) DM for absorption or in thylakoid isolation buffer with 60% (v/v) glycerol (unless otherwise specified) for fluorescence measurements. PBS and PBP samples were diluted in 0.75 M K-phosphate buffer, pH 7.0 [27, 38]. Samples for low-temperature measurements were immersed in liquid nitrogen before and during measurement. Steady-state absorption and low-temperature fluorescence spectra were measured as described [25, 27, 38].

### *2.7 Time-resolved fluorescence spectroscopy, data analysis, and fitting*

TRF measurements were performed at 77 K using a VNF-100 liquid nitrogen cryostat (Janis, USA) and a universal streak-camera system based on the N51716-04 streak tube from Hamamatsu (Hamamatsu Corporation, Japan) and A6365-01 spectrograph from Bruker Corporation (Billerica, MA), coupled to an ultrafast laser system as previously described [43]. The repetition rate of the excitation laser was set to 4 MHz, corresponding to ~250 ns between subsequent pulses. The excitation beam was depolarized, focused on the sample in a circular spot of ~1 mm diameter, and set to a wavelength of 600 nm, with photon flux of $\sim 10^{10}$ photons $cm^{-2}$ per pulse. The emission was measured at a right angle to the excitation beam with a long-pass 610 nm filter placed at the entrance slit of the spectrograph. The integrity of the samples was monitored by observing the photon counts in real-time over the time course of the experiment. When the photon counts were constant, and it was assumed that no sample photodegradation had occurred. The results for whole cells (excitation either into PBP (600 nm) or Chls (410 nm)) were obtained on freshly grown cells. Prior to further analyses, all TRF datasets were subjected to singular-value decomposition (SVD). This mathematical procedure is a least-squares estimator of the original 3D data and is commonly used on large matrixes. Applying the SVD procedure to TRF datasets leads to significant noise reduction [44]. Subsequently, the data were globally fitted with application of a simple fitting model that assumes an irreversible direction of excitation decay from fastest to slowest decaying states. It is commonly called a

sequential model, and spectro-kinetic components obtained from this fitting are commonly called evolution-associated spectra (EAS). We have adapted this nomenclature and refer to such results as evolution-associated fluorescence spectra (EAFS) in order to distinguish them from other types of spectral data (e.g., difference absorption spectra).

### *2.8 Atomic force microscopic imaging of thylakoid membranes*

Thylakoid membranes from *Synechococcus* 7335 cells grown in WL, GL, RL or FRL were prepared and imaged using atomic force microscopy (AFM) as previously described [45], and image processing was performed using Gwyddion v2.47 [46].

## 3.0 Results

### *3.1 Energy transfer in PBS and PBP in* Synechococcus *7335*

PBS and FRL-BCs from cells grown in RL and FRL, respectively were previously purified and characterized for *Synechococcus* 7335 [27, 30]. The same procedures were performed in this study to obtain PBS and FRL-BCs for spectroscopy studies (**Fig. S2**) Cells grown in RL produce hemidiscoidal PBS containing six peripheral rods and tricylindrical cores. The peripheral rods were mostly assembled from PC with trace amounts of PE, and the tricylindrical cores consisted of primarily of allophycocyanin (AP = ApcA1 and ApcB1) and terminal emitter ApcE1, among other subunits (ApcD1, ApcF, ApcC) [27]. In FRL, in addition to the presence of structurally identical RL-type PBS, bicylindrical core (FRL-BC) complexes containing FRL-absorbing AP subunits encoded in FaRLiP gene cluster have also been isolated (**Fig. S2A**; [27]). The steady-state absorbance and low-temperature fluorescence spectral properties of both types of these complexes have also been determined. Under 590-nm excitation at 77 K, RL-PBS had a minor emission at 650 nm from PC but mostly exhibited fluorescence emission at 682 nm from ApcE1 and ApcD1. In contrast, the FRL-BC cores had absorption maxima at 650 and 711 nm and an emission maximum at 730 nm, which presumably emanates from terminal emitters ApcE2 and/or ApcD3 (**Fig. S2B and S2C**; [27, 30]).

Because the FRL-BC cores were only recently discovered and have properties distinct from those of hemidiscoidal PBS synthesized in visible light, comparative analyses are required to characterize these complexes further. TRF was used to analyze purified RL-PBS, FRL-PBS and FRL-BC complexes. The measurements were performed at 77 K to better resolve each fluorescence emission component in these experiments. PBP (mainly PC but also some AP) of RL-PBS were excited with a flash from a femtosecond laser at $\lambda$ = 600 nm, and fluorescence emission was recorded as energy was transferred from PC (emitting at 640-650 nm) to AP (emitting at 660 nm) and finally to the terminal emitters, ApcE1/ApcD1 (emitting at 680 nm) (**Table 1**; **Fig. 1A**). Compared to steady-state fluorescence spectra (**Fig. S2C**), TRF was able to resolve the kinetics of emission increase and decay, and the wavelength resolution was sufficient to distinguish emission from PC or AP. The fluorescence emission and energy transfer kinetics for FRL-PBS were identical to the results for RL-PBS (compare **Figs. 1A** and **1B**). This is consistent with other results showing that RL-PBS and FRL-PBS are structurally and compositionally indistinguishable [27]. Fluorescence emission from PC and AP reached their maxima at ~40 and ~80 ps, respectively, while it requires ~300 ps for the emission from two terminal emitters to reach maximal intensity (**Figs. S3** and **S4**). The emission from PC and AP decayed to half-maximal values within 200 ps and 350 ps, but emission from the terminal emitters continued for up to 2 ns (**Fig. S5**). The results for PBS isolated from cells grown in RL or FRL were nearly identical (data not shown).

The TRF spectra obtained from FRL-BC complexes revealed a previously unknown characteristic of FRL-AP (**Figs. 1C** and **1D**). As previously described [27], the 77-K fluorescence emission maximum for FRL-BC occurs at 730 nm, and this emission was proposed to arise from terminal emitters (ApcE2 and/or ApcD3) (**Fig. S2C**; [27]). However, the fluorescence emission maximum of the bulk FRL-AP (ApcA2/D5-ApcB2) was unknown, because attempts to fractionate components from these complexes have been unsuccessful. The TRF data reveal a component emitting at 720 nm, and the emission from this component rises before the emission at 730 nm from the terminal emitters (**Fig. 1C**). It is known that FRL-BC complexes comprise ApcF, FRL-AP (ApcD5, ApcD2 and ApcB2) and probably two terminal emitters,

ApcE2 and ApcD3 [27]. Because ApcF is also present in RL-PBS and absorbs maximally at ~618 nm, it certainly does not fluoresce at wavelengths longer than 700 nm [47, 48]. Thus, the 720-nm emission likely comes from FRL-AP (i.e., ApcD5, ApcD2 and ApcB2). In the fitting model, the EAFS show the rise and fall of emission at 720 nm that results in the subsequent emission at 730 nm, consistent with energy transfer from FRL-AP to the terminal emitters present in FRL-BC complexes (**Fig. 1D**). The higher resolution TRF spectra for FRL-BC complexes show that the emission at 720 nm reached its maximal value by ~50 ps and decayed to half-maximal intensity by 200 ps, while the maximal emission intensity of the terminal emitters occurred at ~150 ps and decayed to half-maximal value after 800 ps (**Figs. S6 and S7**). These results show that energy transfer to the terminal emitters occurs more rapidly in FRL-BC than in RL-PBS.

### *3.2 Purification and characterization of photosystem II (PSII) in* Synechococcus *7335*

After determining the spectral and TRF properties for RL-PBS and FRL-BC core complexes, we wanted to study further the process of energy transfer from PBS to PSII and PSI in whole cells and from PSII to PSI in thylakoid membranes. However, for accurate interpretation of TRF spectra, it is first necessary to define the sources of all emission features. PSI has previously been isolated and characterized from *Synechococcus* 7335 cells grown in WL and FRL [29]. Due to the similarity of their sizes and sedimentation properties, it is not possible to separate PSI monomers and dimers from PSII dimers on sucrose gradients to obtain highly purified PSII from *Synechococcus* 7335 [14, 29, 49]. Methods for rapid and effective purification of PSII have been established by adding a poly-His-tag to PSII subunits [41, 50] and then employing immobilized metal-affinity chromatography (IMAC) to isolate highly purified PSII complexes.

As described in the **Materials and methods**, a strain expressing $[His]_6$-tagged PsbC2 (i.e., the CP43 subunit encoded in FaRLiP gene cluster) was constructed to allow the purification of FRL-PSII. A scheme showing the design of the construct is presented in **Fig. S1A**. After construction and validation of this strain (**Fig. S1B**), the resulting strain was grown in FRL for more than a month, and cells were harvested for purification of FRL-PSII complexes. The pigment compositions of the wild-type strain and the strain

expressing $[His]_6$-tagged PsbC2 are very similar (**Fig. S8A**). Compared to the wild type, the Chl *d* content of the strain expressing $[His]_6$-tagged PsbC2 was slightly reduced from 1.4% to 1.1% (data not shown), but both values are similar to the percentage of Chl *d* found in thylakoid membranes of the variant strain in FRL (**Table 2**). Due to the fact that the pigment compositions for FRL-PSI and FRL-PSII are different (**Table 2**), these data indicate that the introduction of $[His]_6$-tag into PsbC2 did not change the ratio of FRL-PSI and FRL-PSII very significantly.

The resulting FRL-PSII complexes had highly distinctive spectroscopic properties compared to WL-PSII complexes (**Fig. 2**). The absorption spectra of thylakoid membranes and solubilized thylakoid membranes from FRL-grown cells, as well as the flow-through wash from immobilized metal-affinity chromatography (IMAC) were very similar (**Fig. 2A**). These fractions had a strong absorption band with a maximum at 676 nm and a weaker absorption band at 708 nm. These features presumably are mostly derived from Chl *a* and Chl *f* associated with the more abundant FRL-PSI complexes in these fractions. However, the highly purified FRL-PSII complexes showed very different absorbance features: the $Q_y$ absorbance band for Chl *a* was blue-shifted to 672 nm and a weaker but distinctive absorption band occurred at 723 nm with a shoulder at ~730 nm (**Fig. 2B**). Compared to PSI, the blue-shifted $Q_y$ band for Chl *a* in PSII has been observed in many previous studies and appears to be a common feature of such complexes [51, 52]. The 723-nm absorption maximum is not present in the in the FRL-region of the spectrum of trimeric FRL-PSI [29], but the absorption spectrum is similar to that of FRL-PSII from *Chroococcidiopsis thermalis* PCC 7203 [34] (see **Fig. 2B**).

Three fluorescence emission maxima (683, 714, and 738 nm) were observed for thylakoid membranes, the solubilized thylakoid membranes, and the flow-through eluted from the column during IMAC (**Fig. 2C**). With 440 nm excitation of predominantly Chls, it is obvious that the 683 nm emission comes from WL-PSII and other Chl *a*-binding proteins. The relatively enhanced emission at ~670 nm observed after solubilization of the membranes and wash of the column may indicate that some minor dissociation of Chl *a* from subunits of FRL-PSII or FRL-PSI may have occurred. The origin of the minor emission band at 714 nm is unclear, but it may be the same as the ~720-nm emission feature described

above that is observed for FRL-AP by TRF (**Fig. 1C**) and that is also seen in whole-cell fluorescence spectra [27, 38]. In support of this assignment, a comparison of fluorescence emission spectra for whole cells grown in FRL in the presence or absence of glycerol showed that glycerol treatment enhanced emission at 717 nm (**Fig. S9**). Glycerol treatment of cyanobacterial cells is known to interfere with the integrity of PBS and the energy transfer from PBPs to PSII in cyanobacterial cells [53, 54]. The 738-nm emission represents the emission from FRL-PSI and FRL-PSII. After purification of FRL-PSII complexes by IMAC, highly purified PSII complexes showed a single fluorescence emission band with a maximum at 738 nm (**Fig. 2D**). The purity of this preparation was confirmed by LC-MS/MS analysis of tryptic peptides; only very minor contamination from FRL-PSI was detected, and the PSII subunits encoded by the FaRLiP gene cluster were present as expected (**Table S2**). Pigment analysis showed that FRL-PSII contains Chl *a*, Chl *d*, and Chl *f* (**Table 2**; **Fig. S8A**). Additionally, the FRL-PSII complexes also contained pheophytin (Pheo) *a*, which was identified on the basis of both its absorption spectrum and elution time, but these complexes did not contain Pheo *d* or Pheo *f* (**Fig. S8**). Although FRL-PSII and FRL-PSI have distinctly different pigment compositions and absorption spectra, the low-temperature fluorescence emission maxima of the two complexes are very similar, 738 and 740 nm, respectively (**Fig**. **2D**). However, FRL-PSII does not exhibit the very long-wavelength emission maxima at 803 and 829 nm observed for FRL-PSI [28, 29].

### *3.3 Energy transfer in* Synechococcus *7335 cells grown in RL*

After obtaining the fluorescence emission properties of the three photosynthetic complexes in *Synechococcus* 7335 produced in FRL (**Table 1)**, TRF studies of whole cells and thylakoid membranes from RL and FRL were performed to analyze energy transfer from PBP to PSII and PSI. **Fig. 3** shows TRF results of RL-acclimated *Synechococcus* 7335 whole cells and thylakoid membranes excited at either 410 (excites predominantly Chl) or 600 nm (excites predominantly PBPs; mostly PC but also AP) at 77 K. After excitation at 410 nm, the TRF spectrum is dominated by emission from PSI with a maximum at ~725 nm, but emission from PSII at 685-690 nm is also observed (**Fig. 3A** and **3B**). The results are very different if PBP are excited at 600 nm in whole cells (**Fig. 3C**). Although the 725-nm emission band is still easily

observed because of direct excitation of the $Q_x$ band of Chl *a*, emission bands from PBP (~640 to 660 nm) and PSII (685-690 nm) are enhanced. Emission bands from PBP were also observed when whole cells were excited at 410 nm (**Fig. 3B**), although the emission under these conditions was much weaker. Dissection of the spectra at different time intervals from thylakoid membranes suggests that some excited state energy is transferred from PSII to PSI (**Fig. 3D**). At 100 ps, the spectrum shows two emission peaks from PSII (685-690 nm) and PSI (~725 nm) resulting from excitation of Chl *a*. However, at 240 ps, the emission from PSII decayed while the emission from PSI increased. This result, together with kinetics in thylakoid membranes from RL-grown cells, suggests that at least some direct energy transfer from PSII to PSI occurs in thylakoids (**Figs. 3D** and **S10C**). When excited at 410 nm, the spectra and kinetics for whole cells grown in RL show that the emission from PSII (691 nm) and PSI (725 nm) are maximal at ~90 ps and ~130 ps, respectively, and that the decay half-times for PSII and PSI are ~240 ps and ~570 ps, respectively (**Fig. S10A** and **D**). Because the decreasing emission from PSII is coincident with the rising emission from PSI, these data show that some energy transfer from PSII to PSI also occurs in whole cells. Upon 600-nm excitation, which mainly excites PC in RL-PBS, the emission from 646 nm (PC) is maximal at ~80 ps with a decay half-time of 210 ps. Excitation energy transfer from RL-PBS to PSII (685 nm) and PSI (722 nm) were maximal at 150 ps and 165 ps, respectively, with decay half-times of 400 ps and 880 ps (**Fig. S10B and E**). Although most of the emission from PSI comes from energy transfer from RL-PBS, some emission originates from direct excitation on PSI, as shown in the trace at 65 ps (**Fig. S10B**). These results are consistent with previous results for isolated PBS-PSII-PSI megacomplexes from *Synechocystis* sp. PCC 6803, which showed that energy transfer occurs from PBS to both PSII and PSI, but that the rate from PBS to PSII is faster than that to PSI (however, see also discussion from results of AFM observations below) [11].

In order to extract more insight from the data, a global fitting analysis was performed for both TRF profiles of whole cells (**Fig. 3E** and **3F**). For fitting purposes, a unidirectional (sequential) fitting model was applied. This model does not necessarily provide true fluorescence spectra of molecular species (PSI, PSII, PBS) but rather provides general information about temporal characteristics and time evolution of the

system as a whole. Ideally, it would be most appropriate to build a specific kinetic model that will mimic true excitation migration/decay from "the point of entrance" (PBS) to the final acceptor (PSI). However, this is not possible because it is difficult to predict what happens in the whole cells due to the complexity of excitation energy migration in complex, multi-component systems (various types of free PBPs, intact or partly dissociated PBS, PSII, PSI, etc.). Instead, we provide only general information on the kinetic components that are present in the TRF datasets, and which could be used to infer approximate excitation migration pathways. This method relies upon "evolution-associated fluorescence spectra" (EAFS) that are derived from global analysis of TRF emission data (see **Materials & methods**).

Fitting of the data from 410-nm excitation required only two spectro-temporal components: one is associated with emission from PBS, PSII, and PSI (lifetime 210 ps), and the other is mainly associated with emission from PSI (lifetime 790 ps) (**Fig. 3E**). Energy transfer from PBP/PBS to PSII should largely be complete by 210 ps, but this component will also reflect emission from direct excitation of PSII and PSI. In this respect, the shape of this component resembles emission from thylakoids at 100 ps (**Fig. 3D**). The second component (790 ps lifetime) shows that the emission occurs almost exclusively from PSI. This suggests that at least some energy is transferred from PSII and directly or indirectly from PBP/PBS to PSI. Although emission from PSI is observed for both components and they are similar in shape, the maximum of the second component (790 ps lifetime) is shifted toward longer wavelengths by ~7 nm compared to the first component (210 ps). This indicates that some equilibration probably occurs within the ensemble of Chl *a* molecules in PSI.

In fitting the 600-nm excitation data, one of the fitting components has a fixed lifetime that corresponds to the lifetime of the main PSI-mediated emission while other components can vary (**Fig. 3F**). The fit was reasonably good if three components were used. The first component had an emission band at ~640 nm and a short lifetime of <130 ps, which can be associated with the emission from PC and AP. A second component corresponds to emission from PBP/PBS (PC: 640 nm and AP: 660 nm) that are energetically coupled with PS complexes (PSII: ~685 nm and PSI: ~725 nm). The third component shows

the decay of emissions from PSII and PSI complexes, similar to the results from 410 nm excitation (**Fig. 3E and F**). Collectively, these data indicate that energy is transferred primarily from PC to AP to PSII and/or PSI, but the data indicate that some spillover transfer from PSII to PSI also occurs in cells and thylakoid membranes after growth in RL. These data are completely consistent with results concerning the organization of supercomplexes of PBS, PSII, and PSI in thylakoids from cells grown in RL (see below).

### *3.4 Energy transfer in* Synechococcus *7335 cells grown in FRL*

As mentioned above, there are more fluorescence emission bands at 77 K in *Synechococcus* 7335 in FRL, and the process of energy transfer is therefore potentially more complicated (**Table 1**). When thylakoid membranes were excited at 410 nm at 77 K, three emission bands at 685, 722, and 740 nm were detected after 50 ps (**Fig. 4A** and **4D**). The kinetics suggest that the emission bands at these three wavelengths are probably excited independently (**Fig. S11A** and **S11C**). Residual WL-PSII complexes containing only Chl *a*, or possibly RL-PBS, probably give rise to the weak emission at 685 nm, and the weak emission at 722 nm could potentially come from FRL-BC or WL-PSI complexes that only contain Chl *a*. However, tryptic peptide mass fingerprinting analyses by LC-MS/MS previously showed that subunits from WL-PSI are not very abundant in FRL [29]. Thus, FRL-AP from FRL-BC complexes is probably responsible for the 722 nm fluorescence emission. The 740-nm emission, which is most likely emitted by Chl *f*, could emanate from FRL-PSI, FRL-PSII, or both complexes (**Table 1**). The spectra at selected time intervals show that, as the emission decreased at 685 and 722 nm from 50 to 200 ps, the intensity of emission at 740 nm remain unchanged. These data suggest that excited state energy in WL-PSII and FRL-BC is transferred to FRL-PSII or FRL-PSI (**Fig. 4D**), from which emission then decays up to about 2.3 ns.

When excited at 410 or 600 nm to preferentially excite Chls and PBPs, respectively, *Synechococcus* 7335 whole cells grown in FRL exhibit even more fluorescence emission bands than the corresponding thylakoid membranes (**Fig. 4B, C, E,** and **F**). Five fluorescence emission bands were observed after 410 nm excitation (**Fig. 4B** and **4E**). They occur at 640 nm (PC), 660 nm (AP), 680-690 nm (RL-PBS and WL-

PSII), 720 nm (FRL-AP), and 740 nm (FRL-PSII and FRL-PSI) (**Fig. S11B; Table 1**). The spectra and kinetics of six emission wavelengths from whole cells excited by 410 nm were analyzed. Suggesting that they were excited simultaneously, the emission peaks at 660 and 685 nm were both maximal at ~75 ps and had decay half-times of 200 ps and 260 ps, respectively (**Fig. S11D**). The emission kinetics for the species emitting at 720 nm had slower kinetics, requiring 110 ps to reach maximal intensity and 450 ps to decay to half-maximal intensity. The 740-nm emission had the slowest kinetics, requiring 140 ps to reach maximal intensity with a decay half-time of 660 ps (**Fig. S11D**). In **Fig. S11D**, the 720-nm emission rises more slowly than the emission bands at 685 nm and 740 nm; this is unlike the situation in **Fig. S10C**, in which the emission from WL-PSII (685 nm) and WL-PSI (722 nm) rise simultaneously. These subtle differences suggest that the majority of 722-nm emission in **Fig. S11D** does not arise from WL-PSI but rather comes from FRL-AP. However, the emission at 722 nm overlaps extensively with the much more intense emission peak at 740 nm; this overlap makes the estimation of kinetics for the 722-nm component inaccurate. According to global fitting analysis, during the transition from first component (<150 ps) to second component (430 ps), emission from PC and AP, WL-PBS, WL-PSII, and FRL-AP all decay while the intensity at 740 nm remains constant; this indicates that excitation energy is eventually transferred from all other complexes in the cells to either FRL-PSII or FRL-PSI (**Fig. 4E**).

When *Synechococcus* 7335 whole cells that had been grown in FRL were excited at 600 nm at 77 K, RL-PBS and FRL-BC should be excited predominantly and simultaneously. Six emission bands were observed: 640 nm (PC), 660 nm (AP), 680-690 nm (RL-PBS and WL-PSII), 720 nm (FRL-AP in FRL-BC), 730 nm (terminal emitters in FRL-BC), and 740 nm (FRL-PSII and FRL-PSI) (**Figs. 4C** and **4F**, **S12**, and **S13**). Cells grown in FRL contain both RL (WL) and FRL-types of complexes, which makes the interpretation more complicated, but sequential decays and rises of signals were detected, which facilitated the interpretation of the energy transfer processes. **Figs. S12A** and **S12C** clearly show that mainly two emission peaks at 650 nm and 720 nm were observed at 5 ps, and a third minor emission feature at 680-690 was also visible. The two major emission maxima at ~650 nm (PC in RL-PBS) and 720 nm (FRL-AP in

FRL-BC; see above) indicate that RL-PBS and FRL-BC are independently excited with 600-nm light in cells acclimated to FRL. The weak emission at ~680 nm may come from direct excitation of terminal emitters in RL-PBS or more likely from WL-PSII. Furthermore, the rise-time kinetics for the emissions at 720 nm and 640 nm have nearly the same rates (**Fig. S12B**). The 640-nm emission then migrates to ~660 nm, corresponding to transfer from PC to AP in RL-PBS (**Fig. S12C**). Between 50 and 100 ps, emission from AP begins to decay and emission from the terminal emitters in RL-PBS and WL-PSII at ~680-690 nm becomes maximal. Moreover, at the same time, the emission at 720 nm shifts to 730 nm, which corresponds to energy transfer from FRL-AP to the terminal emitters in the FRL-BC complexes. The observed kinetics are very similar to those observed for these two components in isolated FRL-BC (compare **Figs. S6** and **S12**). The 730-nm peak shifts to 740 nm by 220 ps, which corresponds to energy transfer from FRL-BC to either FRL-PSII, FRL-PSI or both (**Fig. S13**). The decay half-lives at 685 nm and 740 nm are ~400 ps and ~1 ns, respectively, which are longer than the 260 ps and 660 ps half-lives observed under 410 nm excitation. These results show that WL-PSII, FRL-PSII, and FRL-PSI were probably not directly excited with 600-nm excitation and instead received energy by transfer from other complexes (RL-PBS, FRL-BC, and/or FRL-PSII) (**Figs. 4, S12** and **S13**).

Three components were used for global fitting of the TRF spectra for whole cells of *Synechococcus* 7335 grown in RL after 600-nm excitation (**Fig. 4F**). The first component at <140 ps shows emissions from PC (640 nm), AP (660 nm), RL-PBS (680 nm) and FRL-AP (720 nm) (**Fig. 4F**). The second component at 330 ps shows the significant decay of emission from PC and AP in RL-PBS and the rise of emission from terminal emitters in the RL-PBS as well as WL-PSII, the terminal emitters in FRL-BC (ApcE2/ApcD3, 730 nm), and FRL-PSII or FRL-PSI (740 nm) (**Fig. 4F**). The data are consistent with the results for RL-acclimated cells that show energy transfer from RL-PBS to WL-PSII at 685 nm (compare **Figs. 3F** and **4F**). Energy transfer from FRL-AP to the terminal emitters ApcE2/ApcD3 was also shown for isolated FRL-BC complexes (**Fig. 1C** and **1D**). However, it is also possible that energy transfer occurs directly from RL-PBS to FRL-PSII or FRL-PSI (**Fig. 4F**). As shown in **Table S2**, both ApcE1 and ApcE2 copurify to some extent

with FRL-PSII, indicating that individual FRL-PSII complexes may be associated with either RL-PBS or FRL-BC *in vivo*. The third component shows the decay of emissions from WL-PSII, FRL-BC, FRL-PSII, and FRL-PSI complexes (**Fig. 4F**). The half-lifetime of 720 nm emission in FRL-BC is slightly longer in cells (~250 ps) than in purified complexes (~200 ps) (**Figs. S7** and **S13**). This suggests that some of the FRL-AP subunits in cells may not be fully assembled and are energetically uncoupled from downstream energy receivers (FRL-PSII and FRL-PSI).

### *3.5 AFM imaging of Synechococcus 7335 thylakoid membranes*

AFM imaging was performed to examine the distribution of PSI and PSII in thylakoid membranes isolated from cells of *Synechococcus* 7335 grown in RL and FRL (**Figs. 5** and **6**). AFM topographs reveal that PSI complexes occur in at least three distinctive structural arrangements in thylakoids of cells grown in RL (**Figs. 5A-C**, and **6A-C**). In the first arrangement PSI trimers are very closely packed into quasi-regular arrays (**Fig. 5A**), whereas in the second configuration, tightly packed and highly regular arrays of likely PSI dimers are observed (**Fig. 5B; Fig. S14A, B**). These two arrangements occasionally occur in close proximity to one another (**Fig. 5C; Fig. S14C, D**); some of the PSI complexes in **Fig. 5C** may also be monomers. As detected by native gel electrophoresis and sucrose gradient centrifugation, monomeric, dimeric, and trimeric PSI complexes were all observed during purification of PSI from cells grown in WL and RL, with trimeric PSI trimers being the predominant form [29, 36]. The schematic diagram in **Fig. 5D** shows that PSI protrudes on the cytoplasm-facing surface of the thylakoid membrane, which contrasts with the topology of PSII, in which the membrane-extrinsic, water-oxidizing complex protrudes on the lumen-facing surface of the membrane [4, 44].

**Fig. 6** shows a third type of organization for both RL-PSI and RL-PSII, in which the two photosystems form alternating rows of closely packed, monomeric and/or dimeric complexes (**Fig. 6A;** also see **Fig. S15**). The height profile shown in red in **Fig. 6D** corresponds to the dotted red transect in **Fig. 6A**, while the height profile shown in green for RL-PSII complexes corresponds to the dotted green transect in **Fig. 6A**. These profiles correspond to those for PSI (red dotted line) and PSII (green dotted line) as

previously observed [45]. **Fig. 6B** shows a structural model for the organization of the two photosystems in these alternating, row-like arrays. **Fig. 6D** shows the height profiles corresponding to the two dotted-line transects across the thylakoid in **Fig. 6A**, corresponding to PSI (red) and PSII (green). The height profile for the RL-PSII complexes is constant because the cytoplasm-facing surface of PSII is rather flat and feature-less (**Fig. 5D** and **6G**), but the height profile for the PSI complexes shows the characteristic height variation due to the stromal ridge proteins, PsaC, PsaD, and PsaE, of PSI (**Fig. 5D** and **6G**) [3, 45]. **Fig. 6E** shows the same thylakoid patch from panel A, but with two other regions selected that each contain two RL-PSII dimers and four RL-PSI monomers. Transects across the RL-PSI monomers and the corresponding height profiles are shown in **Fig. 6F**. These profiles indicate that the center-to-center distance for these FRL-PSI complexes is about 47 nm. In **Fig. 6G**, the structure of the hemidiscoidal PBS of *Nostoc* sp. PCC 7120 (EMDB code:EMD-2822) has been modeled onto two PSII complexes surrounded by PSI monomers [6]. For these PBS to fit together in the membrane, it is necessary that the PBS in adjacent rows interdigitate slightly; this is possible because of the skewed organization of the PSI-PSII supercomplexes in adjacent rows (**Figs. 6C, 6F** and **6G**). This model can accommodate the slightly wider hemidiscoidal PBS of *Synechococcus* sp. PCC 6803 [27], but it is also possible that the spacing between the rows of complexes might increase in organisms with larger PBS (or that in the absence of PBS for isolated membranes that these complexes become more closely packed). These AFM topographs and models indicate that one PSI monomer is closely associated with each half of a dimeric PSII complex, presumably through an interaction that includes CP47/PsbB in PSII and the PBS core protein ApcD [11]. The model further suggests that these RL-PSI/RL-PSII/PBS supercomplexes might be formed from RL-PSI monomers rather than dimers (although either could be possible). The overall organization of these rows of PSII complexes with attached PBS are similar to the rows of PBS and PSII complexes that have often been observed in thin sections or freeze-fracture images of cyanobacterial and cyanelle thylakoid membranes (**Fig. 6C**; for some examples, see [2, 8, 55-59]). A fourth organization of PSI and PSII probably also exists, in which PSII/PBS supercomplexes [6] form shorter, more disordered rows, around which PSI complexes are likely to be more disordered and interspersed [56, 57]. It is unclear why this type of thylakoid organization is not observed

by AFM, but it could possibly be due to the growth conditions employed, to state transition effects that affect complex organization during membrane isolation, or to the relative binding affinities of the different membrane types to the mica surfaces employed as substrates in AFM.

In contrast to the three arrangements of PSI observed in thylakoids from cells grown in RL, only regular arrays of PSI trimers were observed in thylakoid fragments isolated from cells grown in FRL (**Fig. 5E**). The white dashed line in **Fig. 5E** corresponds to a height profile drawn across the indicated transect across the membrane fragment, which is displayed graphically in **Fig. 5F**. The ~10 nm heights and the periodicity of the topological features resemble those reported for PSI trimers from *Thermosynechococcus elongatus* [45] and for *Synechococcus* 7335 grown in RL (**Fig. 5A**). Although ample evidence for the occurrence of monomeric and dimeric PSI complexes was obtained during the purification and analysis of FRL-PSI [29, 36], trimers were always the predominant form under the isolation conditions employed. Furthermore, the trimeric FRL-PSI complexes seemed to be more stable during purification than trimeric WL-PSI complexes [29, 36]. Finally, no membrane regions similar to those shown in **Fig. 6** or other arrays containing FRL-PSII complexes were observed by AFM.

## 4.0 Discussion

Time-resolved fluorescence spectroscopy (TRF) [11, 33] and AFM [45, 60, 61] are powerful techniques to study the organization and energy transfer characteristics of light-harvesting complexes in photosynthetic organisms. Several TRF analyses have previously been performed in the FaRLiP strain, *H. hongdechloris*, and a Chl *f*-containing cyanobacterium strain KC1, which is also probably a FaRLiP strain [62-64]. Those studies showed that energy transfer from Chl *a* to Chl *f* occurs, and several different emission features were assigned to Chl *f* in these initial studies. However, both Chl *f* and FaRLiP were newly discovered at that time, and detailed analyses of photosynthetic complexes, including analyses with purified FRL-PBP complexes, FRL-PSI, and FRL-PSII, had not yet been performed in *H. hongdechloris* [14, 26-29, 34, 35]. Therefore, to study the overall energy transfer pathway from PBS to PSII and PSI in FRL, we isolated and characterized all of the photosynthetic complexes produced in a single species in FRL

(*Synechococcus* 7335 in this study) and used the information to interpret the results obtained from TRF data and to guide a discussion of possible energy transfer routes in *Synechococcus* 7335 cells grown in RL or FRL. It should be noted that a recent study in *H. hongdechloris* shows uphill energy transfer from Chl *f* to Chl *a* that leads to efficient charge separation [65]. A similar conclusion was derived from determining the action spectrum and relative quantum yield for charge separation in the FRL-PSI complexes of *Synechococcus* 7335 [29].

### *4.1 Models for organization of major light-harvesting complexes and potential energy transfer pathways in* Synechococcus *7335 cells acclimated to RL or FRL*

**Fig. 7** shows models representing the possible organization of the photosynthetic complexes *Synechococcus* 7335 thylakoids and proposed energy transfer pathways in cells acclimated to RL and FRL. The strategy for using RL is similar to that of cyanobacteria that cannot acclimate to FRL (**Fig. 7A**). Arrays of trimeric (**Fig. 7B**) and dimeric PSI (**Fig. 7C**) were observed by AFM in thylakoids membranes from cells grown in RL, and similar arrays of trimeric FRL-PSI were also observed in thylakoids isolated from cells grown in FRL (**Fig. 7D**). It seems likely that in such arrays, only PSI to PSI energy transfer occurs. Light energy absorbed by PC, mainly orange and red wavelengths, is rapidly and efficiently transferred to AP in the core of hemidiscoidal RL-PBS with tricylindrical cores [2, 27]. The energy is then distributed through the terminal emitters, ApcE1 and ApcD1, in the PBS core to WL-PSII and WL-PSI, respectively [6, 9-11]. The TRF measurements also strongly suggest that energy transfer from PSII to PSI also occurs (**Figs. 3, S10,** and **7A**). AFM imaging shows a close association of RL-PSI monomers/dimers and RL-PSII dimers (**Figs. 6** and **S15**). Thus, energy transfer may be facilitated by the formation of RL-megacomplexes, which are here named based on the previously isolated and characterized PBS-PSII-PSI megacomplex of *Synechocystis* sp. PCC 6803 [11].

A megacomplex containing a RL-PBS, a WL-PSII dimer, and two WL-PSI monomers would be enormous, >6 MDa. However, in environments enriched in FRL, the data suggest that three types of megacomplexes could potentially occur in the thylakoids (**Fig. 7E-G**). The first type of complex would

exclusively be assembled from FRL complexes, in which FRL-BC absorbs FRL and transfers the excitation energy to FRL-PSII and FRL-PSI (**Fig. 7E)**. Alternatively, FRL-PSI may associate with RL-PBS and WL-PSII (**Fig. 7F**). In the final case, FRL-BC is replaced by RL-PBS in attachment with FRL-PSII and FRL-PSI (**Fig. 7G**). Note that although FRL-BC or RL-PBS can transfer energy to both PSII and PSI, PSII and PSI can also directly absorb light energy, and arrays containing only FRL-PSI trimers were directly observed by AFM (**Fig. 5E**). Thus, arrays of FRL-PSI trimers also occur as they do in RL (**Figs. 5A, 5D,** and **7B**).

### *4.2 Energy transfer in RL-PBS and FRL- BC*

*Synechococcus* 7335 synthesizes RL-PBS when cells are grown in RL and synthesizes both RL-PBS and FRL-BC in FRL [27, 30]. The steady-state fluorescence emission maximum for FRL-BC at 77 K was previously determined to be 730 nm and was suggested to emanate from two possible terminal emitters, ApcD3 and/or ApcE2 [27, 30]. The TRF results confirmed that the spectral properties and energy transfer characteristics for PBS from cells grown in RL and FRL were identical (**Figs. 1A** and **1B**). A previously unidentified feature at 720 nm was detected in FRL-BC complexes and was assigned as the emission from the bulk FRL-AP (**Figs. 1C**, **S6**, and **S7**). Based on negatively stained preparations in the electron microscope, RL-PBS have six peripheral rods, each containing three hexameric PC disks, but FRL-BC complexes comprise only two core cylinders of FRL-APC without attached peripheral rods (see **Fig. 7**) [27]. Energy transfer to the terminal emitters was faster in FRL-BC (intensity was maximal at ~150 ps) than in RL-PBS (intensity was maximal at ~300 ps). This was probably because of the presence of peripheral PC rods and the one additional AP core cylinder in RL-PBS (**Figs. S3-S7** and **7**). When FRL-BC complexes were directly excited at 600 nm, the emission at 730 nm reached maximal intensity by ~50 ps, faster than the ~80 ps value observed for AP in RL-PBS (**Figs. S3-S7**). The smaller size of the FRL-BC complexes ensures faster energy transfer. Moreover, by eliminating PC and other peripheral rod components that would not be functional in FRL, cells conserve energy, reducing power, and nutrient resources. Finally, the elimination of PC might also reduce light filtering that could prevent light from

reaching other components of the photosynthetic apparatus when the available light is limited (an extreme but natural case of antenna size reduction [66]). Interestingly, cells nevertheless retained some RL-PBS in FRL to allow them to capture RL if it should become available [27].

### *4.3 Properties of PSII in FRL*

This study represents the first time that the fluorescence emission features of the photosynthetic complexes in thylakoids from cells grown in visible light (RL) and FRL have been determined in a single, Chl *f*-containing FaRLiP strain (**Table 1**). PSI and PBP complexes from cells grown in FRL have previously been characterized in *Synechococcus* 7335 [27, 29]. However, highly-purified FRL-PSII is described here for the first time. In contrast to FRL-PSI, FRL-PSII contains Chl *d* and a slightly higher percentage of Chl *f* (4.0% Chl *d* and 12.7% Chl *f*; **Table 2**). These percentages are similar to those for FRL-PSII complexes isolated from *Chroococcidiopsis thermalis* PCC 7203 [34], and they suggest that FRL-PSII complexes contain approximately 1 Chl *d*, 4 Chl *f*, 28 Chl *a*, and 2 Pheo *a* molecules (assuming 35 total Chl-like molecules as found in other PSII complexes [4]).

The differences in the absorption spectra of FRL-PSI and FRL-PSII suggest that the protein environments for Chl *f* are different in the two complexes (**Fig. 2B**) [29]. Nevertheless, the fluorescence emission at low-temperature for FRL-PSI and FRL-PSII are very similar and only differ by 2 nm (**Fig. 2D** and **Table 2**; 740 nm for FRL-PSI and 738 nm for FRL-PSII). At 77 K most of the fluorescence emission from Chl *a*-containing complexes comes from long-wavelength-absorbing Chl species, so-called "red" Chls [66]. The presence of Chl *f* modifies this situation slightly—Chl *f* molecules become "energy traps" and act as the major emitters of fluorescence in the core antenna of PSI and PSII. The emission maxima at 740 and 738 nm show that there are Chl *f* molecules with similarly low energy levels in both FRL-PSI and FRL-PSII, but the fluorescence emissions are unlikely to come from the special pair Chls in these two complexes [29]. Chl *f* species with different emission characteristics were discussed in *H. hongdechloris*, cyanobacterial strain KC1, and *C. thermalis* PCC 7203, although some of the emission features recorded at 630 nm excitation in strain KC1 may have come from PBS in FRL as shown in other species [14, 25, 26,

34, 62-64]. A study in *Acaryochloris marina* suggested that Chl *d* associated with PSII has a major emission band at 728 nm and a weaker emission band at 700 nm [68]. Although those features may also exist in FRL-PSII, they are not observed in steady-state fluorescence spectra. Because the FRL-PSI and FRL-PSII have been purified in *Synechococcus* 7335, it will also be interesting to measure TRF at both 77 K and at room temperature for the purified complexes. In this way, the energy transfer and kinetics of both Chl *f* and Chl *d* molecules from different protein environments can be well-characterized.

### *4.4 The presence of WL-PSII in cells grown in FRL*

Subunits of WL-PSII were detected by tryptic peptide fingerprinting by LC-MS/MS of peptides derived from complexes isolated on sucrose gradients from *Synechococcus* 7335 cells grown in FRL (**Table S2**). Transcriptomic analyses show that relative transcript abundances of paralogous genes encoding PSII subunits in WL do not decrease substantially in FRL within the first 48 h [14, 24, 38, 39]. Steady-state and TRF spectra also indicate the presence of WL-PSII in FRL (**Fig. 3**). The presence of WL-PSII in FRL-acclimated cells has also been confirmed in some other FaRLiP organisms. In *Leptolyngbya* sp. JSC-1 and *Chlorogloeopsis fritschii* PCC 9212, the relative transcript abundances for genes encoding subunits of WL-PSII do not decrease to as great an extent as the genes encoding subunits of WL-PSI, and this process is independent from the regulation of RfpA, RfpB, and RfpC [14, 24, 39]. Although WL-PSII probably cannot efficiently harvest FRL because it only contains Chl *a*, the WL-PSII complexes might serve as docking sites for FRL-BCs that could transfer energy to these complexes. The WL-PSII complexes additional can serve as docking sites to retain RL-PBS, which might therefore maintain some flexibility for harvesting visible light wavelengths when they become available (**Fig. 7F**). This could speed up the transition process for cells acclimated to FRL when they acclimate to visible light again [27, 36]. Whether FRL-BC could dock on WL-PSII complexes is unknown, but if so, then FRL could probably support photochemistry in those complexes.

### *4.5 Energy transfer from WL-PSII to WL-PSI*

The concept of direct energy transfer from PSII to PSI (spillover) in cyanobacteria arose decades ago as a potential mechanism for photoprotection of PSII [69]. More recently, a megacomplex containing PBS, PSII, and PSI was isolated and characterized from *Synechocystis* sp. PCC 6803; this revealed the physical proximity of PSII and PSI and supported the possibility of energy transfer from PBS to both PSI and PSII [11], the pathways for which had been defined by mutations in *apcD* and *apcE/apcF*, respectively, more than 20 years earlier [9, 10]. TRF studies of various species of red algae and cyanobacteria have confirmed the spillover model and show that energy transfer can occur directly from PSII to PSI [70-72]. Spillover also occurs in *Arabidopsis thaliana*, in which energy transfer between PSII and PSI is regulated by light conditions for quenching of excess energy to protect PSII [73]. Based on global analysis of TRF and the coincident decay and rise of fluorescence emission from WL-PSII and WL-PSI, we believe that energy transfer from WL-PSII to WL-PSI occurs in the cyanobacterium *Synechococcus* 7335 (**Figs. 3** and **S10**). Further evidence for spillover can be obtained by measuring TRF of highly purified WL-PSII and WL-PSI complexes and then comparing emission kinetics of the purified complexes with those of whole cells. Finally, the AFM images showing alternating rows of PSI and PSII support the existence of megacomplexes comprising RL-PBS, dimeric WL-PSII, and monomeric WL-PSI in thylakoids (**Fig. 6**).

*Synechococcus* 7335 is a cyanobacterium that is adapted for growth under relatively low light intensities; this is reflected by the observation that its pigment content is greatly reduced under high irradiation (200 μmol photons $m^{-2}$ $s^{-1}$), but this only causes a minimal increase in the growth rate [36]. Therefore, the spillover mechanism in this strain may function as in *A. thaliana* to quench excess energy from PSII under high light conditions [73]. However, this hypothesis will require further validation in *Synechococcus* 7335 by measuring the magnitude of spillover under different growth light intensities and correlating this with relief of photoinhibition under high-light stress conditions.

### *4.6 The pathways of energy transfer in FRL*

Seven fluorescence emission bands are detectable and are well-resolved in TRF spectra in *Synechococcus* sp. PCC 7335 in FRL, representing PC (640 nm), AP (660 nm), the terminal emitters of

RL-PBS (680 nm), WL-PSII (685-695 nm), FRL-AP in FRL-BC (720 nm), terminal emitters ApcD3/ApcE2 in FRL-BC (730 nm), and FRL-PSII and FRL-PSI (738-740 nm) (**Table 1**; **Figs. 4** and **S11-S13**). Excluding the arrays of FRL-PSI alone, we infer that these complexes in FRL may associate in three principal ways: 1. FRL-BC + FRL-PSII + FRL-PSI; 2. RL-PBS + WL-PSII + FRL-PSI; 3. RL-PBS + FRL-PSII + FRL-PSI (**Fig. 7E-G**). Although the emission features of FRL-PSII (738 nm) and FRL-PSI (740 nm) are indistinguishable by TRF, due to the fact that the spillover of energy transfer from WL-PSII to WL-PSI or FRL-PSI occurs in thylakoids of this organism, and the probable proximity of FRL-PSII and FRL-PSI in the thylakoid membrane (**Figs. 5, 6,** and **7A**), it is likely that energy transfer also occurs between FRL-PSII and FRL-PSI (**Figs. 7E** and **7G**). TRF results from excitation at 600 nm support that RL-PBS and FRL-BC transfer energy to FRL-PSI or FRL-PSII (**Figs. 4C** and **F**, **S12**, and **S13**). Peptide analyses showed copurification of ApcE1 and ApcE2 with FRL-PSII complexes (**Table S2**). Although the fluorescence emission bands from FRL-PSI and FRL-PSII are too close to be differentiated in the TRF data, the data suggest that physical interactions occur between FRL-PSII and both RL-PBS and FRL-BC, respectively. Therefore, it is possible that FRL-PSII can receive energy from either RL-PBS or FRL-BC (**Fig. 7E** and **7G**). Although there is no direct evidence showing energy transfer from RL-PBS or FRL-BC to FRL-PSI, given the fact that the organization of complexes in thylakoid membranes in RL supports the presence of megacomplexes (**Fig. 6**), some RL-PBS and FRL-BC seem likely to occur in close proximity with FRL-PSI, which could allow energy transfer to occur (**Fig. 7E-7G**). The indication that energy transfer occurs from RL-PBS and WL-PSII to FRL-PSII and FRL-PSI is important, because this shows that RL-PBS and WL-PSII can possibly function as antenna complexes and transfer energy to FRL-PSII or FRL-PSI to support photochemistry under some growth conditions. At room temperature the energy transferred to Chl *f* in FRL-PSII and FRL-PSI can be efficiently transferred uphill to support charge separation [29, 65]. This could provide FRL-acclimated cells with some flexibility to utilize any incidental visible light that reaches their niches. This organization also supports uninterrupted photochemistry when cells must reverse-acclimate from FRL to visible light.

Due to the complexity of the photosynthetic apparatus in FRL, further genetic modifications may be required to study energy transfer solely between and among FRL complexes. ApcE is the core-membrane linker that organizes the structure of the core cylinder complexes in both FRL-BC (ApcE2) and RL-PBS (ApcE1) complexes [2, 5]. Generating individual knockout mutants for *apcE1* or *apcE2* should efficiently disrupt the assembly and downstream energy transfer for RL-PBS or FRL-BC in FRL. This would simplify the composition of photosynthetic apparatus in FRL and will greatly assist in understanding could further simplify the available pathways for energy transfer. Construction of these and other knock-out mutants is in progress.

## 5. Conclusion

*Synechococcus* 7335 is the first strain for which all photosynthetic complexes (PSI, PSII, and PBS) produced in FRL have been highly purified and characterized [27, 29, 36; this study]. This information greatly assisted in the interpretation of energy transfer among those complexes by TRF. TRF successfully deconvoluted the fluorescence emission associated with two populations of AP in FRL-BC and showed that emission at 720 nm occurs predominantly from the major AP population (presumably that formed by ApcD5 and ApcB2) in FRL-BC [27]. By using both thylakoid membranes and whole cells for TRF studies, we analyzed the energy transfer pathways in RL and FRL conditions. In cells grown in RL, energy is transferred from RL-PBS to both WL-PSII and WL-PSI, and direct evidence for (PBS)-PSII-PSI megacomplexes was obtained by AFM. However, spillover energy transfer from WL-PSII to WL-PSI was also observed. In cells grown in FRL, five photosynthetic complexes were detected (RL-PBS, WL-PSII, FRL-BC, FRL-PSII, and FRL-PSI). Combining results from proteomics analysis by tryptic peptide fingerprinting, complex isolation, and TRF, we suggest the existence of three types of megacomplexes in FRL: (1) FRL-BC, FRL-PSII, and FRL-PSI; (2) RL-PBS, WL-PSII, and FRL-PSI; (3) RL-PBS, FRL-PSII, and FRL-PSI. No matter what overall organization of complexes exists, the TRF results indicate that energy is eventually transferred to FRL-PSI complexes. This suggests that visible light captured in those complexes in FRL can also be transferred to FRL-PSII or FRL-PSI for support photochemistry. By retaining some

complexes that harvest visible light in FRL-acclimated cells, cyanobacteria gain the flexibility to use both visible light and FRL. This flexibility would be highly advantageous in supporting rapid reverse acclimation of FRL-acclimated cells to the use of visible light.

**Transparency document**

The Transparency document associated with this article can be found, in online version.

**Acknowledgments**

This research was conducted under the auspices of the Photosynthetic Antenna Research Center (PARC), an Energy Frontier Research Center funded by the DOE, Office of Science, Office of Basic Energy Sciences under Award Number DE-SC 0001035. This work was also supported by the National Science Foundation grant MCB-1613022 to D.A.B. Work in the laboratory of C.N.H. was supported by Advanced Award 338895 from the European Research Council which funded C.M.-C., and provided partial support for C.N.H. C.N.H. also gratefully acknowledges financial support from the Biotechnology and Biological Sciences Research Council (BBSRC UK), award number BB/M000265/1. M.-Y.H. gratefully acknowledges a travel award from PARC that allowed him to travel to Washington University in St. Louis to use the PARC spectroscopy facilities to perform the time-resolved fluorescence studies described herein.

**Author contributions**

M.-Y.H. designed and performed research, analyzed and interpreted data, and wrote and edited the manuscript. D.A.B. obtained the funding for the research, directed the research, assisted in interpretation of the results, and wrote and edited the manuscript. D.M.N. performed TRF spectroscopy, analyzed and interpreted the spectroscopic data, and edited the manuscript. C.M.-C. performed the AFM studies, interpreted the results, constructed models, and prepared figures. C.N.H. provided financial support for the AFM studies, interpreted the AFM data, and assisted in preparing the figures and manuscript. G.G. performed the trypsin digestion and proteomics analysis and assist in the revision of the manuscript. R.E.B.

obtained the funding for the research and contributed to the interpretation of the data and the revision of the manuscript.

## Conflict of interest statement

The authors declare that the research was conducted in the absence of any commercial or financial relationships that could be construed as a potential conflict of interest.

## Appendix A. Supplementary data

Supplementary data for this article can be found online at https://XXXXXX.

**References**


[1] D.A. Bryant (Ed.), *The Molecular Biology of Cyanobacteria, Advances in Photosynthesis and Respiration,* Vol. 1, Springer (1994) 892 pp., Dordrecht, The Netherlands.

[2] D.A. Bryant, D.P. Canniffe, How nature designs light-harvesting antenna systems: design principles and functional realization in chlorophototrophic prokaryotes, J. Phys. B: At. Mol. Opt. Phys. 51 (2018) 033001.

[3] I. Grotjohann, P. Fromme, P. Structure of cyanobacterial photosystem I, Photosynth. Res. 85 (2005) 51–72.

[4] Y. Umena, Y., K. Kawakami, J.-R. Shen, N. Kamiya, Crystal structure of oxygen-evolving photosystem II at a resolution of 1.9 Å, Nature 473 (2011) 55–60.

[5] W. Sidler, in *Advances in Photosynthesis and Respiration*, Vol. 1, *The Molecular Biology of Cyanobacteria* (D.A. Bryant, Ed.), Springer (1994), pp. 139–216, Dordrecht, The Netherlands.

[6] L. Chang, X. Liu, Y. Li, C.-C. Liu, F. Yang, J. Zhao, S.-F. Sui, Structural organization of an intact phycobilisome and its association with photosystem II, Cell Res. 25 (2015) 726–737.

[7] A.N. Glazer, Light guides. Directional energy transfer in a photosynthetic antenna, J. Biol. Chem. 264 (1989) 1–4.

[8] D.A. Bryant, G. Guglielmi, N. Tandeau de Marsac, A. M. Castets, G. Cohen-Bazire, The structure of cyanobacterial phycobilisomes: A model. Arch. Microbiol. 123 (1979), 113–127.

[9] J. Zhao, J. Zhou, D.A. Bryant, Energy transfer processes in phycobilisomes as deduced from analyses of mutants of *Synechococcus* sp. PCC 7002. In: *Research in Photosynthesis,* Vol. I (N. Murata, Ed.), Kluwer (1992), pp. 25–32, Dordrecht, The Netherlands.

[10] C. Dong, A. Tang, J. Zhao, C.W. Mullineaux, G. Shen, D.A. Bryant, ApcD is necessary for efficient energy transfer from phycobilisomes to photosystem I and helps to prevent photoinhibition in the cyanobacterium *Synechococcus* sp. PCC 7002, Biochim. Biophys. Acta 1787 (2009) 1122–1128.

[11] H. Liu, H. Zhang, D.M. Niedzwiedzki, M. Prado, M., G. He, M.L. Gross, R.E. Blankenship, Phycobilisomes supply excitations to both photosystems in a megacomplex in cyanobacteria, Science 342 (2013) 1104–1107.

[12] M. Chen, M. Schliep, R.D. Willows, Z.-L. Cai, B.A. Neilan, H. Scheer, A red-shifted chlorophyll, Science 329 (2010) 1318–1319.

[13] M. Chen, Y. Li, D. Birch, D., R.D. Willows, A cyanobacterium that contains chlorophyll *f*- a red-absorbing photopigment, FEBS Lett. 586 (2012) 3249–3254.

[14] F. Gan, S. Zhang, N.C. Rockwell, S.S. Martin, J.C. Lagarias, D.A. Bryant, Extensive remodeling of a cyanobacterial photosynthetic apparatus in far-red light, Science 345 (2014) 1312–1317.

[15] L. Behrendt, A. Brejnrod, M. Schliep, S.J. Sørensen, A.W.D. Larkum, M. Kühl, Chlorophyll *f*-driven photosynthesis in a cavernous cyanobacterium, ISME J. 9 (2015) 2108–2111.

[16] F. Gan, D.A. Bryant, Adaptive and acclimative responses of cyanobacteria to far-red light, Environ. Microbiol. 17 (2015) 3450–3465.

[17] E. Trampe, M. Kühl, Chlorophyll *f* distribution and dynamics in cyanobacterial beachrock biofilms, J. Phycol. 52 (2016) 990–996.

[18] S. Ohkubo, H. Miyashita, A niche for cyanobacteria producing chlorophyll *f* within a microbial mat. ISME J. 11 (2017) 2368–2378.

[19] Z.-C. Zhang, Z.-K. Li, Y.-C. Yin, Y. Li, Y. Jia, M. Chen, B.-S. Qiu, Widespread occurrence and unexpected diversity of red-shifted chlorophyll producing cyanobacteria in humid subtropical forest ecosystems. Environ. Microbiol. (2019) in press.

[20] C. Gómez-Lojero, L.E. Leyva-Castillo, P. Herrera-Salgado, J. Barrera-Rojas, E. Ríos-Castro, E.B. Gutiérrez-Cirlos, *Leptolyngbya* CCM 4, a cyanobacterium with far-red photoacclimation from Cuatro Ciénegas Basin, México. Photosynthetica 56 (2018) 342–353.

[21] R.L. Airs, B. Temperton, C.Sambles, G. Farnham, S.C. Skill, C.A. Llewellyn, Chlorophyll *f* and chlorophyll *d* are produced in the cyanobacterium *Chlorogloeopsis fritschii* when cultured under natural light and near-infrared radiation. FEBS Lett. 588 (2014) 3770–3777.

[22] F. Gan, G. Shen, G., D.A. Bryant, Occurrence of far-red light photoacclimation (FaRLiP) in diverse cyanobacteria, Life 5 (2015) 4–24.

[23] M.-Y. Ho, N.T. Soulier, D. P. Canniffe, G. Shen, D.A. Bryant, Light regulation of pigment and photosystem biosynthesis in cyanobacteria, Curr. Opin. Plant. Biol. 37 (2017) 24–33.

[24] C. Zhao, F. Gan, G. Shen, D.A. Bryant, RfpA, RfpB, and RfpC are the Master Control Elements of Far-Red Light Photoacclimation (FaRLiP), Front. Microbiol. 6 (2015) 1303.

[25] M.-Y. Ho, G. Shen, D.P. Canniffe, C. Zhao, D.A. Bryant, Light-dependent chlorophyll *f* synthase is a highly divergent paralog of PsbA of Photosystem II. Science 353 (2016) aaf9178.

[26] Y. Li, Y. Lin, C.J. Garvey, D. Birch, R.W. Corkery, P.C. Loughlin, H. Scheer, R.D. Willows, M. Chen, Characterization of red-shifted phycobilisomes isolated from the chlorophyll *f*-containing cyanobacterium *Halomicronema hongdechloris*. Biochim. Biophys. Acta 1857 (2016) 107–114.

[27] M.-Y. Ho, F. Gan, G. Shen, D.A. Bryant, Far-red light photoacclimation (FaRLiP) in *Synechococcus* sp. PCC 7335. II. Characterization of phycobiliproteins produced during acclimation to far-red light, Photosynth. Res. 131 (2017) 187–202.

[28] G. Shen, D.P. Canniffe, M.-Y. Ho, V. Kurashov, A. van der Est, J.H. Golbeck, D.A. Bryant, Characterization of chlorophyll *f* synthase heterologously produced in *Synechococcus* sp. PCC 7002, Photosynth. Res. (2019) in press, doi: 10.1007/s11120-018-00610-9.

[29] V. Kurashov, M.-Y. Ho, G. Shen, K. Piedl, T.N. Laremore, D.A. Bryant, J.H. Golbeck, Characterization of Photosystem I and II complexes isolated from cyanobacteria grown in far-red light, Photosynth. Res. (2019) in press, doi: 10.1007/s11120-019-00616-x

[30] P. Herrera-Salgado, L.E. Leyva-Castillo, E. Rios-Castro, C. Gómez-Lojero, Complementary chromatic and far-red photoacclimation in *Synechococcus* ATCC 29403 (PCC 7335). The phycobilisomes, a proteomic approach, Photosynth. Res. 138 (2018) 39–56.

[31] T. Gillbro, Å. Sandström, V. Sundström, J. Wendler, A.R. Holzwarth, (1985) Picosecond study of energy-transfer kinetics in phycobilisomes of *Synechococcus* 6301 and the mutant AN 112, Biochim. Biophys. Acta 808 (1985) 52–65.

[32] C.W. Mullineaux, A.R. Holzwarth, Kinetics of excitation energy transfer in the cyanobacterial phycobilisome-Photosystem II complex, Biochim. Biophys. Acta 1098 (1991) 68–78.

[33] S. Akimoto, M. Yokono, How light-harvesting and energy-transfer processes are modified under different light conditions: studies by time-resolved fluorescence spectroscopy, in *Photosynthesis: Structures, Mechanisms, and Applications,* H.J.M. Hou, M.M. Najafpour, G.F. Moore, S.I. Allakhverdiev (Eds.)*,* Springer International Publishing (2017) pp. 169–184, Berlin.

[34] D.J. Nürnberg, J. Morton, S. Santabarbara, A. Telfer, P. Joliot, L.A. Antonaru, A.V. Ruban, T. Cardona, E. Krausz, A. Boussac, A. Fantuzzi, A.W. Rutherford, Photochemistry beyond the red limit in chlorophyll *f*–containing photosystems, Science 360 (2018) 1210–1213.

[35] Y. Li, Y., N. Vella, M. Chen, Characterization of isolated photosystem I from *Halomicronema hongdechloris*, a chlorophyll *f*-producing cyanobacterium, Photosynthetica 56 (2018) 306–315.

[36] M.-Y. Ho, Characterization of far-red photoacclimation in cyanobacteria, Ph. D. thesis, The Pennsylvania State University (2018).

[37] R. Rippka, J. Deruelles, J.B. Waterbury, M. Herdman, R.Y. Stanier, Generic assignments, strain histories and properties of pure cultures of cyanobacteria, Microbiology 111 (1979) 1–61.

[38] M.-Y. Ho, F. Gan, G. Shen, C. Zhao, D.A. Bryant, Far-red light photoacclimation (FaRLiP) in *Synechococcus* sp. PCC 7335: I. Regulation of FaRLiP gene expression, Photosynth. Res. 131 (2017) 173–186.

[39] M.-Y. Ho, D.A. Bryant, Global transcriptional profiling of the cyanobacterium *Chlorogloeopsis fritschii* PCC 9212 in far-red light: insights into the regulation of chlorophyll *d* biosynthesis, Front. Microbiol. 10 (2019) 465.

[40] M. Sugiura, Y. Inoue, Highly purified thermo-stable oxygen-evolving photosystem II core complex from the thermophilic cyanobacterium *Synechococcus elongatus* having His-tagged CP43, Plant Cell Physiol. 40 (1999) 1219–1231.

[41] Y. Zhao, Y. Shi, W. Zhao, X. Huang, D. Want, N. Brown, J. Brand, J. Zhao, CcbP, a calcium-binding protein from *Anabaena* sp. PCC 7120, provides evidence that calcium ions regulate heterocyst differentiation. Proc. Natl. Acad. Sci. USA 102 (2005) 5744–4748.

[42] T. Sakamoto, T., D.A. Bryant, Growth at low temperature causes nitrogen limitation in the cyanobacterium *Synechococcus* sp. PCC 7002, Arch. Microbiol. 169 (1998) 10–19.

[43] D.M. Niedzwiedzki, J. Jiang, C.S. Lo, R.E. Blankenship, Low-temperature spectroscopic properties of the peridinin–chlorophyll *a*–protein (PCP) complex from the coral symbiotic dinoflagellate *Symbiodinium*. J. Phys Chem. B 117 (2013) 11091–11099.

[44] E.R. Henry, J. Hofrichter, Singular value decomposition — application to analysis of experimental data, Meth. Enzymol. 210 (1992) 129–192.

[45] C. MacGregor-Chatwin, M. Sener, M.S.F. Barnett, A. Hitchcock, M.C. Barnhart-Dailey, K. Maghlaoui, J. Barber, J.A. Timlin, K. Schulten, C.N. Hunter, Lateral segregation of photosystem I in cyanobacterial thylakoids. Plant Cell 29 (2017) 1119–1136.

[46] D. Nečas, P. Klapetek, Gwyddion: an open-source software for SPM data analysis. *Open Physics* 10 (2012) 181–188.

[47] D.A. Bryant, R. de Lorimier, G. Guglielmi, S.E. Stevens, Jr., Structural and compositional analyses of the phycobilisomes of *Synechococcus* sp. PCC 7002. Analyses of the wild-type strain and a phycocyanin-less mutant constructed by interposon mutagenesis. Arch. Microbiol. 153 (1990) 550–560.

[48] M.K. Ashby, C.W. Mullineaux, The role of ApcD and ApcF in energy transfer from phycobilisomes to PS I and PS II in a cyanobacterium, Photosynth. Res. 61 (1999) 169–179.

[49] G. Shen, J. Zhao, S.K. Reimer, M.L. Antonkine, Q. Cai, S.M. Weiland, J.H. Golbeck, D.A. Bryant, Assembly of photosystem I: I. Inactivation of the *rubA* gene encoding a membrane-associated rubredoxin in the cyanobacterium *Synechococcus* sp. PCC 7002 causes a loss of photosystem I activity, J. Biol. Chem. 277 (2002) 20343–20354.

[50] M. Sugiura, Y. Inoue, J. Minagawa, Rapid and discrete isolation of oxygen-evolving His-tagged photosystem II core complex from *Chlamydomonas reinhardtii* by $Ni^{2+}$ affinity column chromatography, FEBS Lett. 426 (1998) 140–144.

[51] M. Rögner, P.J. Nixon, B.A. Diner, Purification and characterization of photosystem I and photosystem II core complexes from wild-type and phycocyanin-deficient strains of the cyanobacterium *Synechocystis* PCC 6803, J. Biol. Chem. 265 (1990) 6189–6196.

[52] G.R. Wolfe, F.X. Cunningham, B. Grabowski, E. Gantt, Isolation and characterization of Photosystems I and II from the red alga *Porphyridium cruentum*, Biochim. Biophys. Acta 1188 (1994) 357–366.

[53] G. Shen, S. Boussiba, W.F. Vermaas, *Synechocystis* sp PCC 6803 strains lacking photosystem I and phycobilisome function, Plant Cell 5 (1993) 1853–1863.

[54] H.-B. Mao, G.-F. Li, D.-H. Li, Q.-Y. Wu, Y.-D. Gong, X.-F. Zhang, N.-M. Zhao, Effects of glycerol and high temperatures on structure and function of phycobilisomes in *Synechocystis* sp. PCC 6803, FEBS Lett. 553 (2003) 68–72.

[55] T.H. Giddings, Jr., C. Wasmann, L.A. Staehelin, Structure of the thylakoids and envelope membranes of the cyanelles of *Cyanophora paradoxa*, Plant Physiol. 71 (1983) 409–419.

[56] J. Olive, G. I. M'Bina, C. Vernotte, C. Astier, F.-A. Wollman, Randomization of the EF particles in thylakoid membranes of Synechocystis 6714 upon transition from state 1 to state 2, FEBS Lett. 208 (1986) 203–212.

[57] J. Olive, G. Ajlani, C. Astier, M. Recouvreur, C. Vernotte, Ultrastructure and light adaptation of phycobilisome mutants of *Synehocystis* PCC 6803. Biochim. Biophys. Acta 1319 (1986) 275–282.

[58] D.V. Zlenko, P.M. Krasilnikov, I.N. Stadnichuk, Structural modeling of the phycobilisome core and its association with the photosystems. Photosynth. Res. 130 (2016) 347–356.

[59] D.V. Zlenko, T.V. Golochkina, P.M. Krasilnikov, I.N. Stadnichuk, Coupled rows of PBS cores and PSII dimers in cyanobacteria, Photosynth. Res. 133 (2017) 245–260.

[60] J.N. Sturgis, J.D. Tucker, J.D. Olsen, R.A. Niederman, Atomic force microscopy studies of native photosynthetic membranes, Biochemistry 48 (2009) 3679–3698.

[61] L.-N. Liu, S. Scheuring, Investigation of photosynthetic membrane structure using atomic force microscopy, Trends Plant Sci. 18 (2013) 277–286.

[62] T. Tomo, T. Shinoda, M. Chen, S.I. Allakhverdiev, S. Akimoto, S. Energy transfer processes in chlorophyll *f*-containing cyanobacteria using time-resolved fluorescence spectroscopy on intact cells, Biochim. Biophys. Acta 1837 (2014)1484–1489.

[63] S. Akimoto, Shinoda, M.Chen, S.I. Allakhverdiev, T. Tomo, Energy transfer in the chlorophyll *f*-containing cyanobacterium, *Halomicronema hongdechloris*, analyzed by time-resolved fluorescence spectroscopies, Photosynth. Res. 125 (2015) 115–122.

[64] S. Itoh, T. Ohno, T. Noji, H. Yamakawa, H. Komatsu, K. Wada, M. Kobayashi, H. Miyashita, Harvesting far-red light by chlorophyll *f* in photosystems I and II of unicellular cyanobacterium strain KC1, Plant Cell Physiol. 56 (2015) 2024–2034.

[65] F.-J. Schmitt, Z.Y. Campbell, M.V. Bui, A. Hüls, T. Tomo, M. Chen, E.G. Maksimov, S.I. Allakhverdiev, T. Friedrich, Photosynthesis supported by a chlorophyll *f*-dependent, entropy-driven uphill energy transfer in *Halomicronema hongdechloris* cells adapted to far-red light, Photosynth. Res. 139 (2018) 185–201.

[66] H. Kirst, C. Formighieri, A Melis, Maximizing photosynthetic efficiency and culture productivity in cyanobacteria upon minimizing the phycobilisome light-harvesting antenna size, Biochim. Biophys. Acta 1837 (2014) 1653–1664.

[67] N.V. Karapetyan, E. Schlodder, R. van Grondelle, J.P. Dekker, The long wavelength chlorophylls of photosystem I, in *Advances in Photosynthesis and Respiration*, Vol. 24, *Photosystem I* (J.H. Golbeck, Ed.), 2006, pp. 177–192, Springer, Berlin.

[68] T. Tomo, Y. Kato, T. Suzuki, S. Akimoto, T. Okubo, T. Noguchi, K. Hasegawa, T. Tsuchiya, K. Tanaka, M. Fukuya, N. Dohmae, T. Watanabe, M. Mimuro, Characterization of highly purified photosystem I complexes from the chlorophyll *d*-dominated cyanobacterium *Acaryochloris marina* MBIC 11017, J. Biol. Chem. 283 (2008) 18198–18209.

[69] J. Biggins, D. Bruce, Regulation of excitation energy transfer in organisms containing phycobilins, Photosynth. Res. 20 (1989) 1–34.

[70] M. Yokono, A. Murakami, S. Akimoto, S. Excitation energy transfer between photosystem II and photosystem I in red algae: Larger amounts of phycobilisome enhance spillover, Biochim. Biophys. Acta 1807 (2011) 847–853.

[71] N. Kowalczyk, F. Rappaport, C. Boyen, F.-A. Wollman, J. Collén, P. Joliot, Photosynthesis in *Chondrus crispus*: The contribution of energy spill-over in the regulation of excitonic flux, Biochim. Biophys. Acta 1827 (2013) 834–842.

[72] Y. Ueno, S. Aikawa, A. Kondo, S. Akimoto, Energy transfer in cyanobacteria and red algae: confirmation of spillover in intact megacomplexes of phycobilisome and both photosystems, J. Phys. Chem. Lett 7 (2016) 3567–3571.

[73] M. Yokono, A. Takabayashi, S. Akimoto, A. Tanaka, A megacomplex composed of both photosystem reaction centres in higher plants, Nat. Commun. 6 (2015) 6675.

**Table 1.** Characteristic features in 77-K fluorescence emission spectra for each photosynthetic complex from *Synechococcus* 7335 cells grown in RL or FRL. The emission features are summarized from published results [27, 29] and from this study. If known, the protein subunit or complex associated with each emission band is provided in parentheses.

| Growth light | Complex | Fluorescence emission band (nm) |
|---|---|---|
| RL | PBS | 640 (PC)<br>660 (AP)<br>682 (ApcE1/ApcD1) |
| | PSII | 684, 693 (PsbC, PsbB) |
| | PSI | 723 |
| FRL | PBS | 640 (PC)<br>660 (AP)<br>682 (ApcE1/ApcD1) |
| | BC | ~720 (ApcD5/ApcB2)<br>730 (ApcE2/ApcD3) |
| | PSII | 684, 693 (WL-PSII)<br>738 (FRL-PSII) |
| | PSI | 740 |

**Table 2.** Chlorophyll compositions of thylakoid membranes from cells grown in FRL, trimeric FRL-PSI, and FRL-PSII. The pigment composition of each sample was analyzed by RP-HPLC, and the percentage of each pigment was estimated based on the absorbance of each Chl at 680 nm as previously described [28]. The standard deviation was calculated from three independent biological replicates.

| | Chl *d* | Chl *f* | Chl *a* |
|---|---|---|---|
| FRL thylakoids | 1.2 ± 0.1% | 8.2 ± 0.4% | 90.6 ± 0.5% |
| FRL-PSI trimers | 0.3 ± 0.1% | 7.7 ± 0.6% | 92.0 ± 0.7% |
| FRL-PSII | 4.0 ± 0.7% | 12.7 ± 0.6% | 83.3 ± 1.2% |

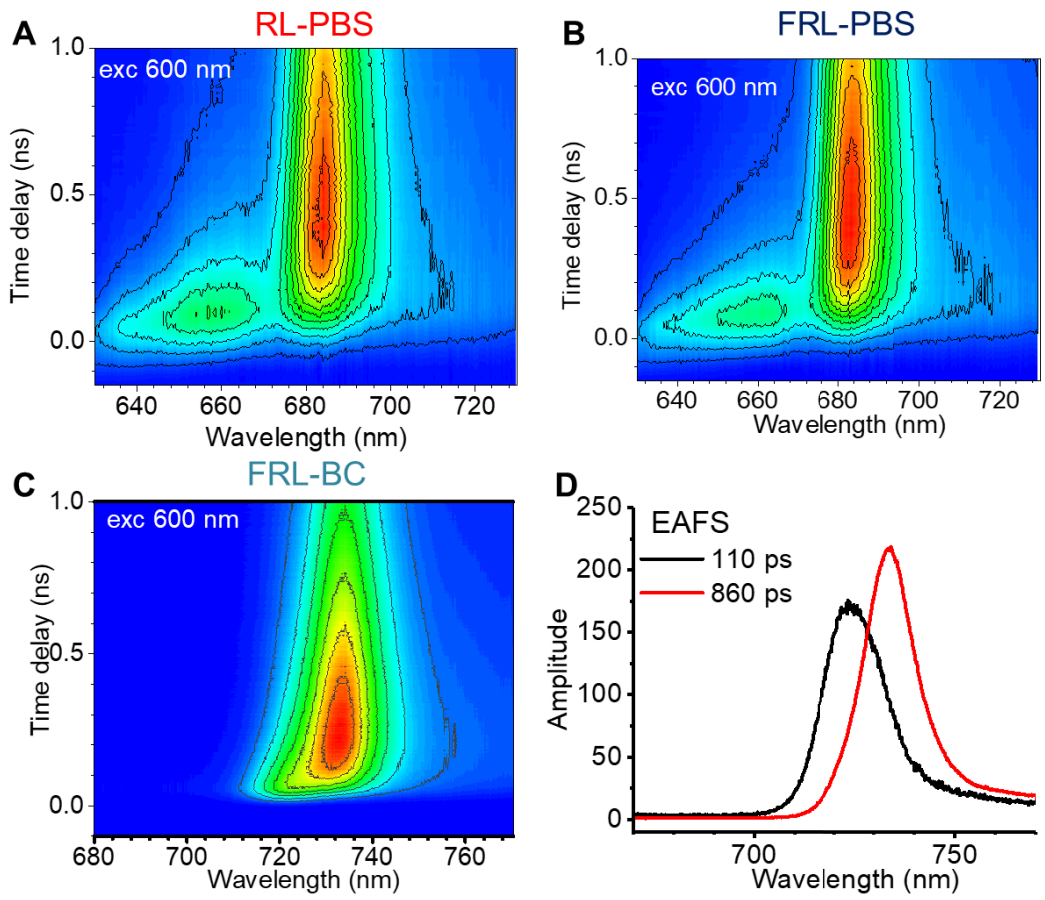


**Fig. 1.** Time-resolved fluorescence spectroscopy (TRF) at 77 K of PBS from *Synechococcus* 7335 cells grown in RL (RL-PBS), PBS from cells grown in FRL (FRL-PBS), and bicylindrical cores from cells grown in FRL (FRL-BC). The isolation of these three fractions from sucrose gradient centrifugation and their steady-state absorption and fluorescence emission spectra are shown in **Fig. S2**. All samples were excited at 600 nm to excite PBPs preferentially (mostly PC but also AP), the time range for data collections was from 0 to 1.0 ns, and the data were collected at 77K. The color in the 3D-pseudocolor diagram corresponds to the intensity of fluorescence emission. The gradient of intensity changes from lowest level in blue shades to the highest levels in red shades. (A) TRF fluorescence emission spectra of RL-PBS, (B) TRF fluorescence emission spectra of FRL-PBS, and (C) TRF fluorescence emission spectra of FRL-BC. (D) Results of global fitting (EAFS) of the TRF dataset from panel C.

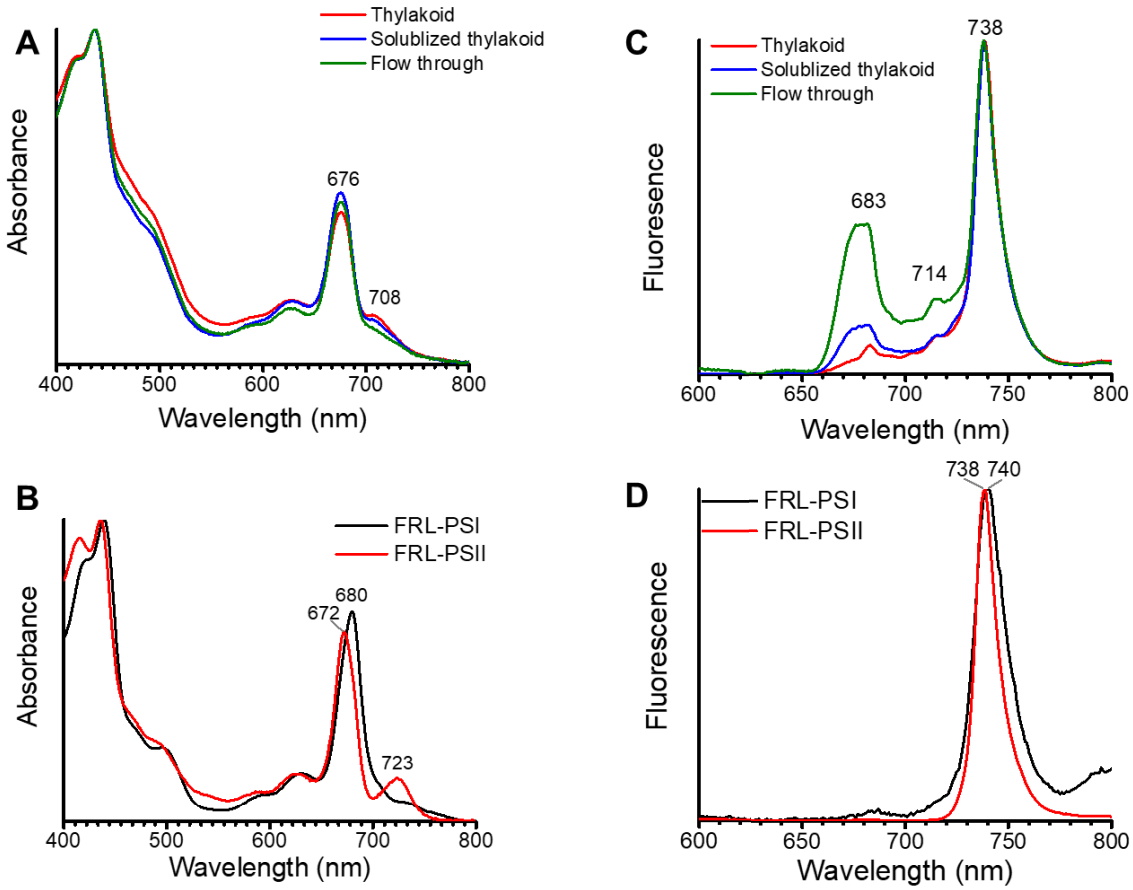


**Fig. 2.** Absorption and 77-K fluorescence emission spectra obtained during purification of FRL-PSII from *Synechococcus* 7335. *Synechococcus* 7335 strain expressing $[His]_6$-tagged *psbC2* were grown in FRL for more than one month and used as the starting material for purification of FRL-PSII. Absorption and 77-K fluorescence emission spectra (excitation at 440 nm) were taken from isolated thylakoids, solubilized thylakoids, and the flow-through (wash from IMAC during column purification), and the imidazole elution fraction containing purified FRL-PSII. (A) Absorption spectra and (C) 77-K fluorescence emission spectra for thylakoid membranes, solubilized thylakoid membranes, and flow-through fractions. (B) Absorption spectra and (D) 77-K fluorescence emission spectra of purified FRL-PSII (red line) and FRL-PSI (black line) [29].

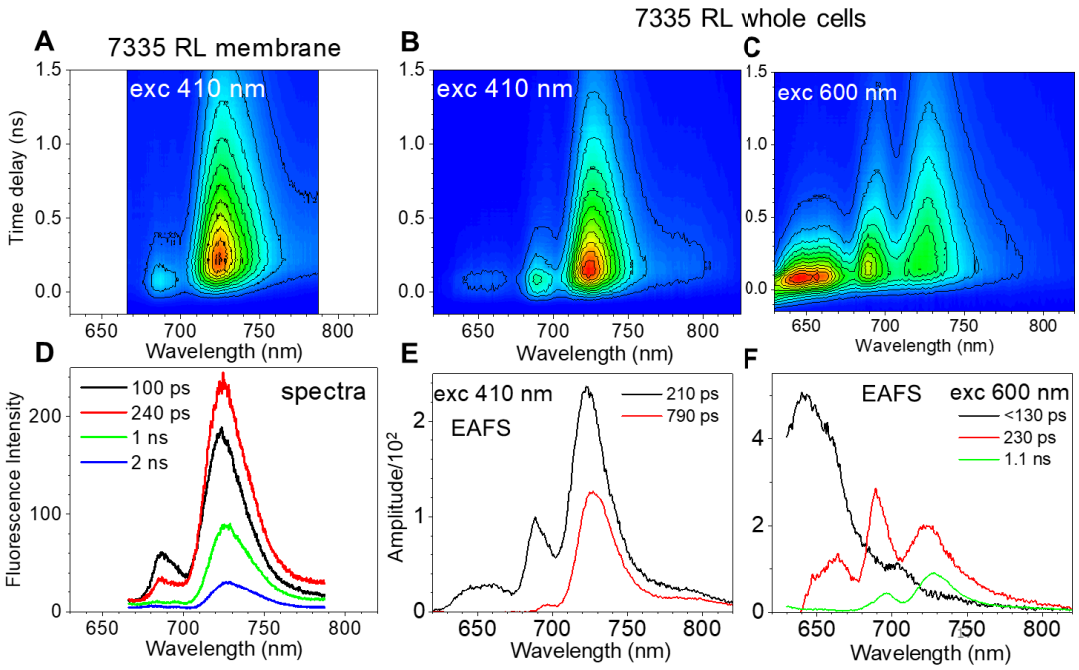


**Fig. 3.** Time-resolved fluorescence emission spectra of thylakoid membranes and whole cells of RL-acclimated *Synechococcus* 7335 excited at 410 (preferentially excites Chl *a*) and 600 nm (preferentially excites PBP, mostly PC) at 77 K. The top panels (A-C) show 3D-pseudocolor representation of TRF results in the time range from 0 to 1.5 ns. The gradient of intensity changes from lowest levels in blue shades to the highest levels in red shades. (A) thylakoid membranes from RL-grown cells excited at 410 nm; (B) whole cells grown in RL excited at 410 nm; (C) whole cells grown in RL at excited 600 nm. (D) Examples of fluorescence emission spectra for thylakoid membranes excited at 410 nm taken at the indicated delay times with respect to excitation at time 0. (E and F) Global fitting results from application of a sequential decay model (EAFS) for excitation of *Synechococcus* 7335 whole cells grown in RL excited at 410 nm (E) and 600 nm (F). Two spectro-kinetic components were sufficient to fit the data from 410-nm excitation and three components from 600-nm excitation. Decay lifetimes of the EAFS are provided. For additional details, see text. For additional details, see text.

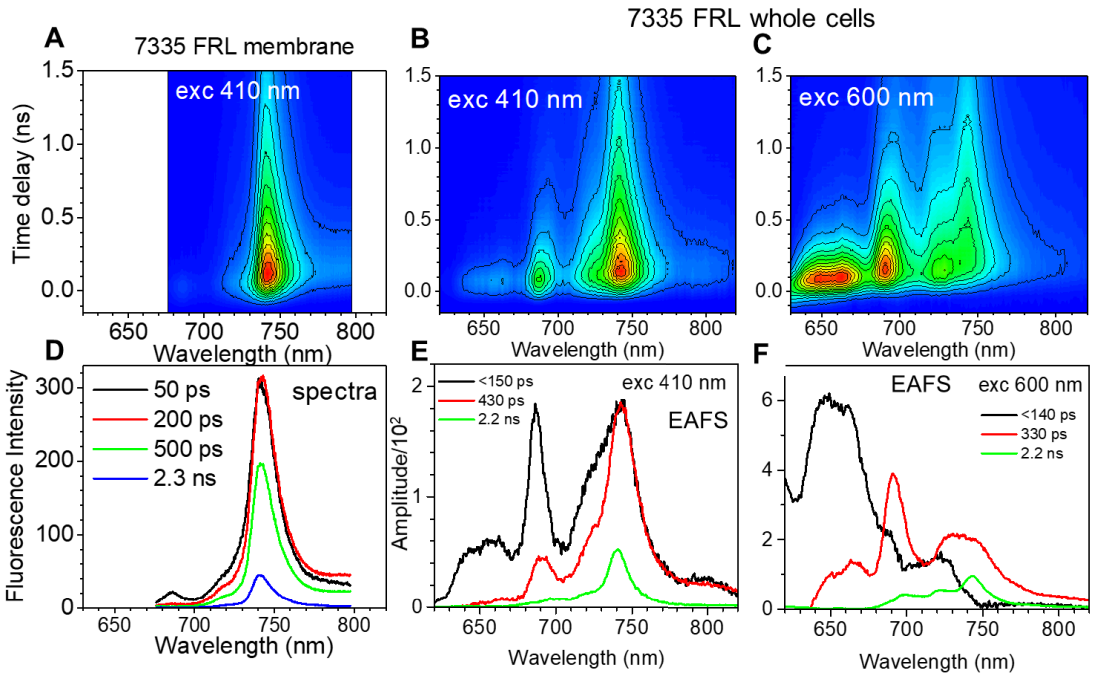


**Fig. 4.** Time-resolved fluorescence emission spectra of thylakoid membranes and whole cells of FRL-acclimated *Synechococcus* 7335 excited at 410 (preferentially excites Chl *a*) and 600 nm (preferentially excites PBP) at 77 K. The top panels (A-C) show 3D-pseudocolor representation of TRF results in the time range from 0 to 1.5 ns. The gradient of intensity changes from lowest levels in blue shades to the highest levels in red shades. (A) thylakoid membranes from FRL-grown cells excited at 410 nm; (B) whole cells grown in FRL excited at 410 nm; (C) whole cells grown in FRL excited at 600 nm. (D) Examples of fluorescence emission spectra for thylakoid membranes excited at 410 nm taken at the indicated delay times with respect to excitation at time 0. Global fitting results (EAFS, evolution associated fluorescence spectra) from application of a sequential decay model to TRF data for whole cells of *Synechococcus* 7335 grown in RL after excitation at 410 nm (E) and 600 nm (F). For additional details, see text.

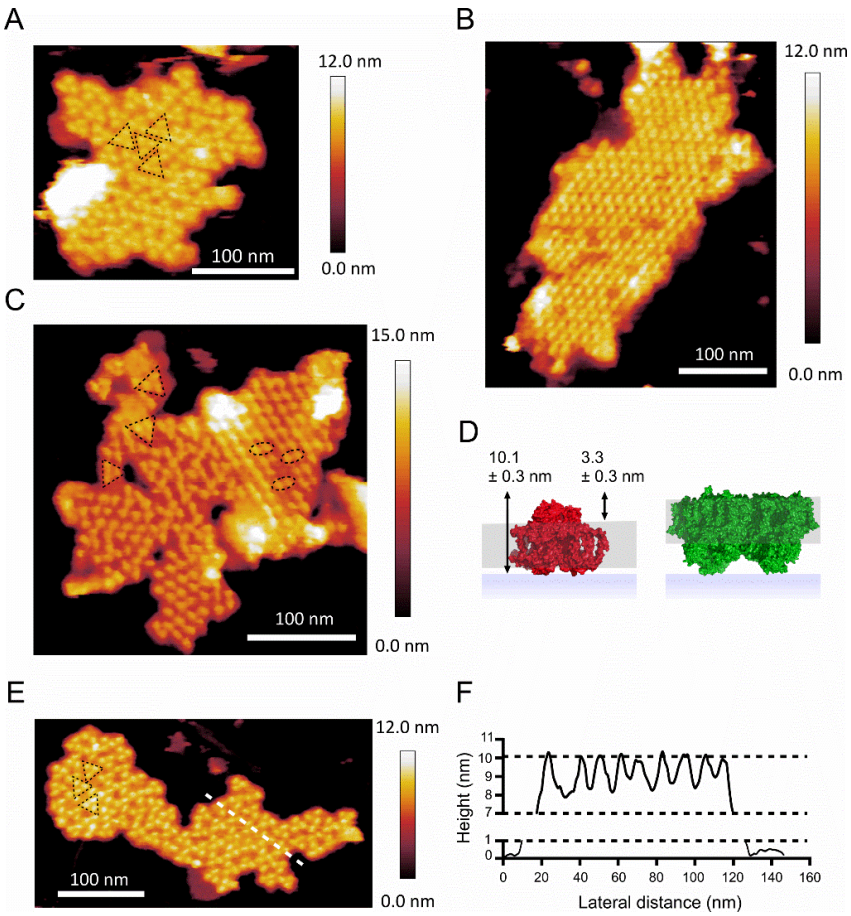


**Fig. 5.** Two types of organization for PSI complexes in thylakoid membranes isolated from *Synechococcus* 7335 cells grown in RL or FRL. (A) AFM topograph of a thylakoid membrane patch from *Synechococcus* 7335 acclimated to RL, showing areas of disorganized PSI trimers, four of which are delineated in black. These trimers are not in a pseudo-crystalline organization as previously described [45] (B) Topograph of a membrane patch from RL acclimated *Synechococcus* 7335 showing a large array of PSI complexes, likely in a dimeric configuration. The dimensions of these complexes are consistent with the trimeric PSI crystal structure. (C) Topograph of a thylakoid membrane from RL acclimated *Synechococcus* 7335 where both PSI configurations are present. Three trimers and three putative dimers are delineated in black. (D) Schematic diagram illustrating the protrusions of PSI (red; PDB code:1JB0) and the lack of PSII (green; PDB code:3WU2) protrusions on the cytoplasmic face of the membrane; the heights of the PSI complex above the lipid bilayer (grey) and the mica surface (blue) measured from the AFM data are shown. (E) Thylakoid membrane patches from *Synechococcus* 7335 acclimated in FRL, showing an array of trimeric complexes similar in organization to those shown in panel A. The dashed white line shows the position of a section used for the height profile in (F). (F) Height profile corresponding to the white dashed line in

panel (E), showing the heights of a series of trimeric complexes with respect to the supporting mica substrate. See **Fig. S14** for additional topographs.

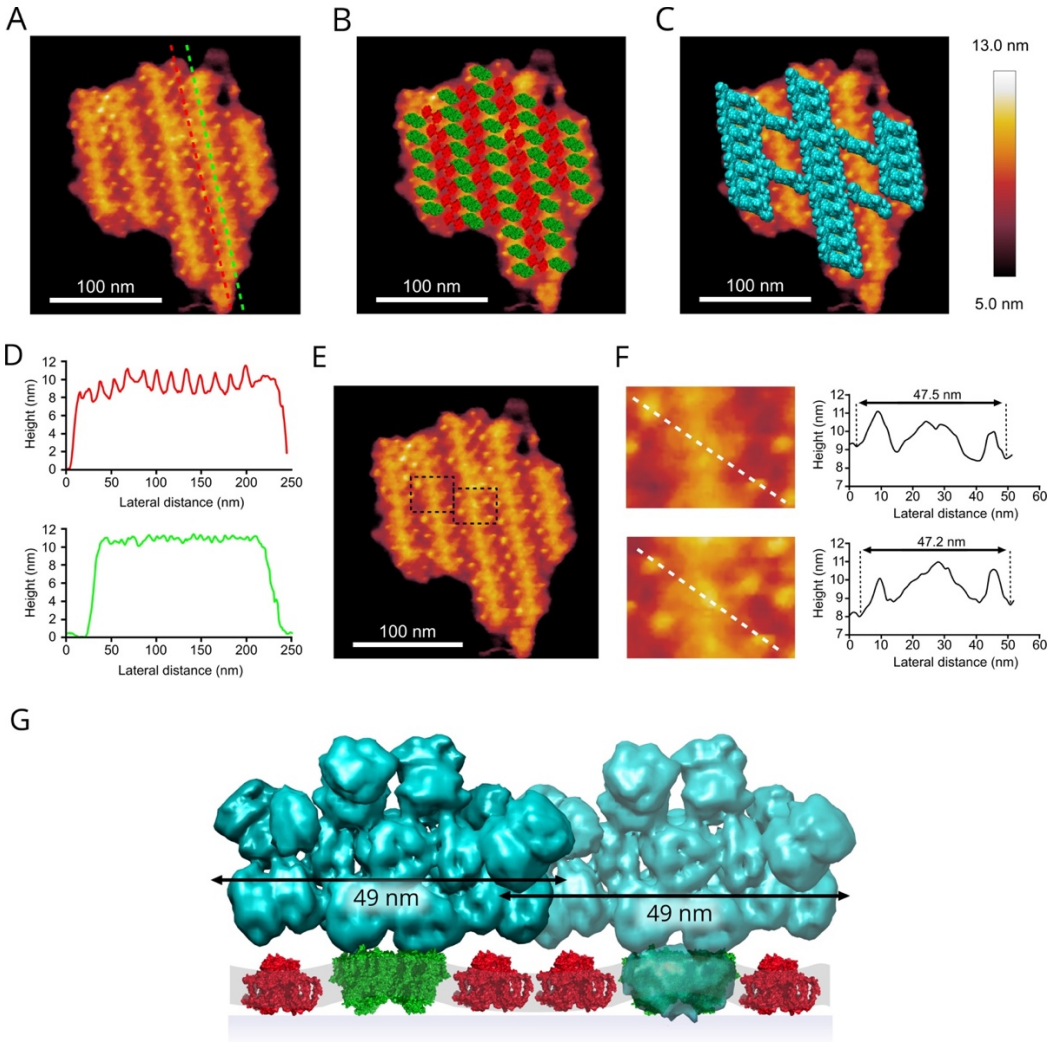


**Fig. 6.** The organization of PSI and PSII in thylakoid membranes from *Synechococcus* 7335 cells grown in RL. (A) AFM topograph showing a thylakoid membrane from RL acclimated *Synechococcus* 7335 showing alternating rows of topology, assigned to dimeric PSI and dimeric PSII complexes. A PSI monomer can be visualized as a single topological feature due to the cytoplasmic protrusion formed by the PsaC, PsaD, PsaE subunits, whereas PSII appears as a somewhat amorphous feature owing to the lack of cytoplasmic protrusions in this complex (see Fig. 5D). (B) The same topograph shown in (A) with the paired PSI monomers (PDB code:1JB0) and dimeric PSII complexes (PDB code:3WU2) fitted to the AFM data. (C) The same topograph as shown in (A) with the hemidiscoidal PBS structure from *Nostoc* sp. PCC 7120 (PDB code:5Y6P) [6] overlaid to show how these large, extrinsic antenna complexes could assemble along the PSI and PSII rows. (D) Height profiles corresponding to the red and green dashed lines in (A) showing the cytoplasmic protrusions of the PSI complexes (top red profile) and the minimal cytoplasmic protrusions of the PSII complexes (bottom green profile). The same topograph as shown in (A) with two selected regions (boxes) that each contain four monomeric RL-PSI complexes and the equivalent of two RL-PSII

complexes. These selected regions are enlarged in panel (F) and the height profiles corresponding to the dotted white-line transects extending across two PSI monomers are shown. The center-to-center distance between the RL-PSI monomers is ~47 nm. See **Fig. S15** for additional topographs. (G) Schematic showing the proposed assembly of PSI, PSII and PBS in RL-acclimated *Synechococcus* 7335. PSI and PSII protrude to differing extents on the lumenal side of the membrane; the diagram shows how the planarity of the thylakoid membrane could be distorted by adhesion of PSI and PSII to the mica substrate. In the left-hand PBS the PSII complex portion of the PBS-PSII structure (EMDB code:EMD-2822) determined by Chang et al. [6] has been omitted; on the right side, the PSII complex from the PBS-PSII structure has been retained and the transparent image is overlaid on the green PSII model, to show how the overlay was used to position the PBS in order to merge the PBS-PSII structure with the model and reconcile this structure with distances measured from the AFM topograph. The 49-nm maximum width of each PBS, indicated by a black arrow, roughly corresponds to the ~47-nm PSI-PSII-PSI periodicity measured by AFM. Also shown in this figure, the skewed positions of PSII in the adjacent rows leads to a slightly interdigitating arrangement of adjacent PSII-PBS complexes, which allows for the very tight packing that can be observed in panel 6C.

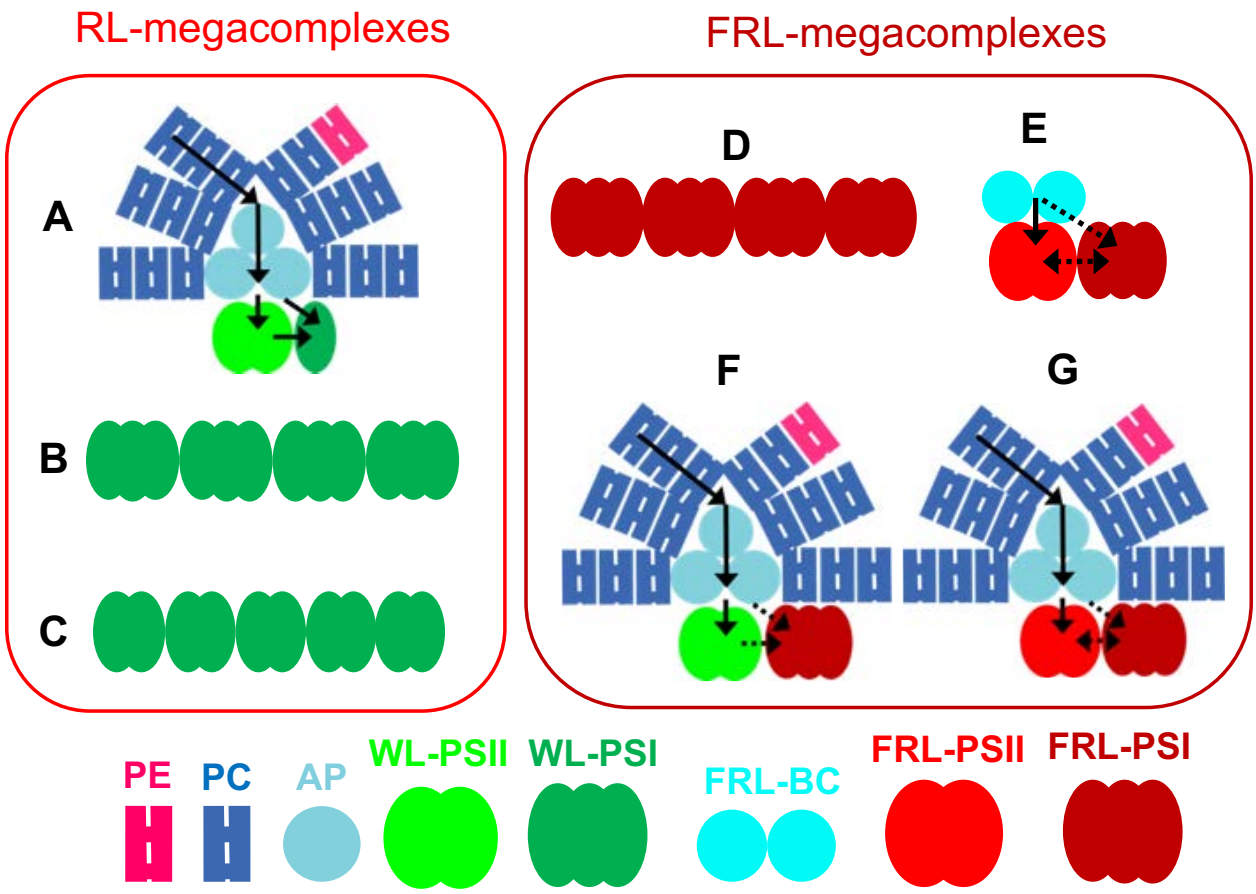


**Fig.7.** Scheme showing possible organization of photosynthetic complexes and routes of energy transfer in cells of *Synechococcus* 7335 acclimated to RL and FRL. Color coding and naming of complexes is shown at the bottom of the figure: phycoerythrin (PE); phycocyanin (PC); allophycocyanin (AP); Chl *a*-associated PSII dimer (WL-PSII); Chl *a*-associated PSI trimer (WL-PSI); FRL-absorbing bicylindrical core (FRL-BC); PSII dimer associated with Chl *a*, Chl *d*, and Chl *f* (FRL-PSII); PSI trimer associated with Chl *a* and Chl *f* (FRL-PSI). (A-C) Possible assemblies of complexes and routes of excitation energy transfer in cells acclimated to RL and involving (A) megacomplexes consisting of RL-PBS, WL-PSII dimer, and WL-PSI monomer; (B) array of WL-PSI trimers; and (C) array of WL-PSI dimers. (D-G) Possible routes of excitation energy transfer in cells acclimated to FRL and three possible megacomplex assemblies: (D) array of FRL-PSI trimers; (E) FRL-BC, FRL-PSII, and FRL-PSI; (F) RL-PBS, WL-PSII, and FRL-PSI; (G). RL-PBS, FRL-PSII, and FRL-PSI. The actual organization of FRL-PSII and FRL-PSI is uncertain, as no supporting AFM images have yet been obtained. However, it is possible that complexes similar to those in FRL might exist in FRL.

**SUPPLEMENTARY TABLES S1 and S2 AND FIGURES S1-S15**

# Extensive remodeling of the photosynthetic apparatus alters energy transfer among photosynthetic complexes when cyanobacteria acclimate to far-red light

**Ming-Yang Ho[a,b,1], Dariusz M. Niedzwiedzki[c], Craig MacGregor-Chatwin[d], Gary Gerstenecker[c], C. Neil Hunter[d], Robert E. Blankenship[c,e], and Donald A. Bryant[a,b,f]***

[a]*Department of Biochemistry and Molecular Biology, The Pennsylvania State University, University Park, PA USA*

[b]*Intercollege Graduate Program in Plant Biology, The Pennsylvania State University, University Park, PA USA*

[c]*Department of Energy, Environmental & Chemical Engineering and Center for Solar Energy and Energy Storage, Washington University, St. Louis, MO USA*

[d]Department of Molecular Biology and Biotechnology, University of Sheffield, Sheffield UK

[e]*Departments of Biology and Chemistry, Washington University, St. Louis, MO USA*

[f]*Department of Chemistry and Biochemistry, Montana State University, Bozeman, MT USA*

[1]Present address: Plant Research Laboratory, Michigan State University, MI USA

***Address for Correspondence:** Dr. Donald A. Bryant, S-002 Frear Laboratory, Department of Biochemistry and Molecular Biology, The Pennsylvania State University, University Park, PA 16802 USA. Phone; 814-865-1992; Fax: 814-863-7024; E-mail: dab14@psu.edu

**Table S1 Sequences of primers used for generation of constructs for introducing the sequence of [His]$_6$-tag at the C-terminus of *psbC2* in *Synechococcus* 7335, and primers for PCR analysis to confirm segregation of transconjugants.** Introduced restriction sites are underlined, the sequence of [His]$_6$-tag is double-underlined, and numbered primers are annotated in **Fig. S1**.

| | |
|---|---|
| P1: XhoI_psbC2His_u_F | 5'-AGATCTCGAGTGGAGCCAGTCAAATTCAGC-3' |
| P2: XmaI_psbC2His_u_R | 5'-AGCCCGGGGTCAGAACGCAAGCTCGGAT-3' |
| P3: XmaI_His_Km_F | 5'-ACCCCGGGCTGGTACCACGCGGTTCTCACCAC CACCACCACCACTAGCACGCTGCCGCAAGCACT-3' |
| P4: SalI_Km_R | 5'-GCTGTCGACGGTGGGCGAAGAACTCCAG-3' |
| P5: SalI_psbC2His_d_F | 5'-ACCGTCGACAGCTAGCATCGGCTGCATCC-3' |
| P6: SacI_psbC2His_d_R | 5'-CGCGAGCTCTAATATTCTAATGCACCCAT-3' |
| P7: psbC2His_u_F | 5'-GCCTGCGAAAAAGTTTGTTTTCCCC-3' |
| P8: psbC2His_d_R | 5'-GTGAAACCTTTGTCATCGCCT-3' |

**Table S2 Mass spectrometric identification indicates the purity of FRL-PSII in *Synechococcus* 7335**. Protein compositions in solubilized thylakoid membranes (Thylakoid) and purified FRL-PSII were identified by LC-MS/MS of tryptic peptides. Bold font indicates the subunits of PSI, PSII, and PBS cores that are encoded within the FaRLiP gene cluster. Exclusive spectrum count indicates counts of spectra of specific peptides detected for the specified individual proteins.

| PS I Gene | Locus tag | Exclusive Spectrum Count | |
|---|---|---|---|
| | | **FRL-PSII** | **Thylakoid** |
| *psaA1* | S7335_1678 | 0 | 5 |
| ***psaA2*** | **S7335_5506** | **7** | **55** |
| *psaB1* | S7335_3312 | 0 | 6 |
| ***psaB2*** | **S7335_4329** | **12** | **53** |
| *psaC*[1] | NZ_DS989904 (621310-621552) | | |
| *psaD* | S7335_2287 | 15 | 83 |
| *psaE* | S7335_5210 | 7 | 34 |
| *psaF1* | S7335_4059 | 0 | 7 |
| ***psaF2*** | **S7335_5139** | **4** | **61** |
| *psaI1* | S7335_1386 | | |
| ***psaI2*** | **S7335_2282** | | |
| *psaJ1* | S7335_4019 | 0 | 0 |
| ***psaJ2*** | **S7335_5198** | | |
| *psaK* | S7335_5488 | | |
| *psaL1* | S7335_2406 | 0 | 0 |
| ***psaL2*** | **S7335_2771** | **0** | **24** |
| *psaM*[1] | NZ_DS989904 (3715842-3715934) | | |
| PS II Gene | Locus tag | Exclusive Spectrum Count | |
| | | **FRL-PSII** | **Thylakoid** |
| *psbA* | S7335_2623 | 4 | 4 |
| *psbA* | S7335_1528 | | |
| *psbA-r*[3] | S7335_524 | | |
| *psbA* | S7335_157 | | |
| ***psbA3*** | **S7335_4273** | **147** | **21** |
| ***chlF*** | **S7335_4253** | | |
| *psbB1*[1,2] | NZ_DS989904 (2482009-2481290) | | |
| ***psbB2*** | **S7335_4830** | **403** | **100** |
| *psbC1* | S7335_4424 | 3 | 18 |
| ***psbC2*** | **S7335_3753** | **569** | **99** |

| | | | |
|---|---|---|---|
| *psbD1*[2] | S7335_5047 | | |
| *psbD2* | S7335_1444 | 138 | 56 |
| ***psbD3*** | **S7335_2548** | **186** | **60** |
| *psbE* | S7335_3478 | | |
| *psbF1* | S7335_3021 | | |
| *psbF2* | S7335_3212 | | |
| *psbH1*[1] | NZ_DS989904 (4700131-4700311) | | |
| ***psbH2*** | **S7335_1601** | **41** | **8** |
| *psbI* | S7335_3454 | | |
| *psbJ* | S7335_2707 | | |
| *psbK* | S7335_3963 | | |
| *psbL* | S7335_1441 | | |
| *psbN* | S7335_5602 | | |
| *psbO1* | S7335_5307 | 75 | 76 |
| *psbO2* | S7335_4784 | 18 | 39 |
| *psbP* | S7335_1471 | 8 | 18 |
| *psbQ* | S7335_2036 | 8 | 65 |
| *psbT*[1] | NZ_DS989904 (2480084-2479992) | | |
| *psbU* | S7335_3378 | | |
| *psbV1* | S7335_4926 | | |
| *psbV2* | S7335_1375 | | |
| *psbW* | S7335_2558 | 73 | 24 |
| *psbX* | S7335_4754 | | |
| *psbY* | S7335_1446 | | |
| *psbZ* | S7335_4595 | | |
| *psb27* | S7335_5437 | 4 | 6 |

| PBS Gene | Locus tag | Exclusive Spectrum Count | |
|---|---|---|---|
| | | **FRL-PSII** | **Thylakoid** |
| *apcA1* | S7335_4074 | 14 | 81 |
| ***apcA2/D5*** | **S7335_4229** | **113** | **234** |
| *apcB1* | S7335_4775 | 61 | 93 |
| ***apcB2*** | **S7335_2392** | **168** | **266** |
| *apcB3* | S7335_1338 | | |
| *apcC* | S7335_3276 | | |
| *apcD1* | S7335_2013 | 0 | 6 |
| ***apcD2*** | **S7335_3274** | **64** | **41** |
| ***apcD3*** | **S7335_4445** | **70** | **63** |
| *apcD4* | S7335_2899 | | |
| *apcE1* | S7335_1839 | 94 | 100 |
| ***apcE2*** | **S7335_3294** | **254** | **163** |
| *apcF* | S7335_1487 | 31 | 44 |

| | | | |
|---|---|---|---|
| *cpcA1* | S7335_1630 | 1 | 37 |
| *cpcA2* | S7335_2244 | 0 | 23 |
| *cpcB1* | S7335_3505 | 1 | 42 |
| *cpcB2* | S7335_4452 | 1 | 38 |
| *cpcH/I* | S7335_4519 | 7 | 13 |
| *cpcH/I* | S7335_4033 | 8 | 21 |
| *cpcD* | S7335_3524 | | |
| *cpcE* | S7335_2363 | 0 | 5 |
| *cpcF* | S7335_4405 | | |
| *cpcG* | S7335_2387 | 1 | 5 |
| *cpcG* | S7335_4257 | | |
| *cpcS* | S7335_4321 | | |
| *cpcT* | S7335_2352 | | |
| *cpeA* | S7335_2962 | | |
| *cpeB* | S7335_2684 | 0 | 6 |
| *cpeC* | S7335_2087 | | |
| *cpeD* | S7335_3667 | 0 | 6 |
| *cpeR* | S7335_1781 | | |
| *cpeE* | S7335_2235 | 1 | 4 |
| *cpeS* | S7335_2433 | | |
| *cpeT* | S7335_3658 | | |
| *cpeV* | S7335_4282 | | |
| *cpeU* | S7335_3548 | | |
| *cpeY* | S7335_3216 | | |
| *cpeZ* | S7335_3652 | | |
| *pcyA1* | S7335_1677 | | |
| *pcyA2* | S7335_1843 | | |
| *pebA* | S7335_1967 | | |
| *pebB* | S7335_3562 | | |
| *nblA* | S7335_4089 | | |
| *nblA* | S7335_3920 | | |
| *petH* | S7335_1472 | | |

[1]This gene is present in draft genome, but it was not auto-annotated, and the results were not individually calculated.

[2]The DNA sequences of the *psbB1* and *psbD1* genes are incomplete in the draft genome and thus results could not be individually calculated.

[3]*r-* "*r-psbA*" indicates the "rogue" *psbA* gene (S7335_524).

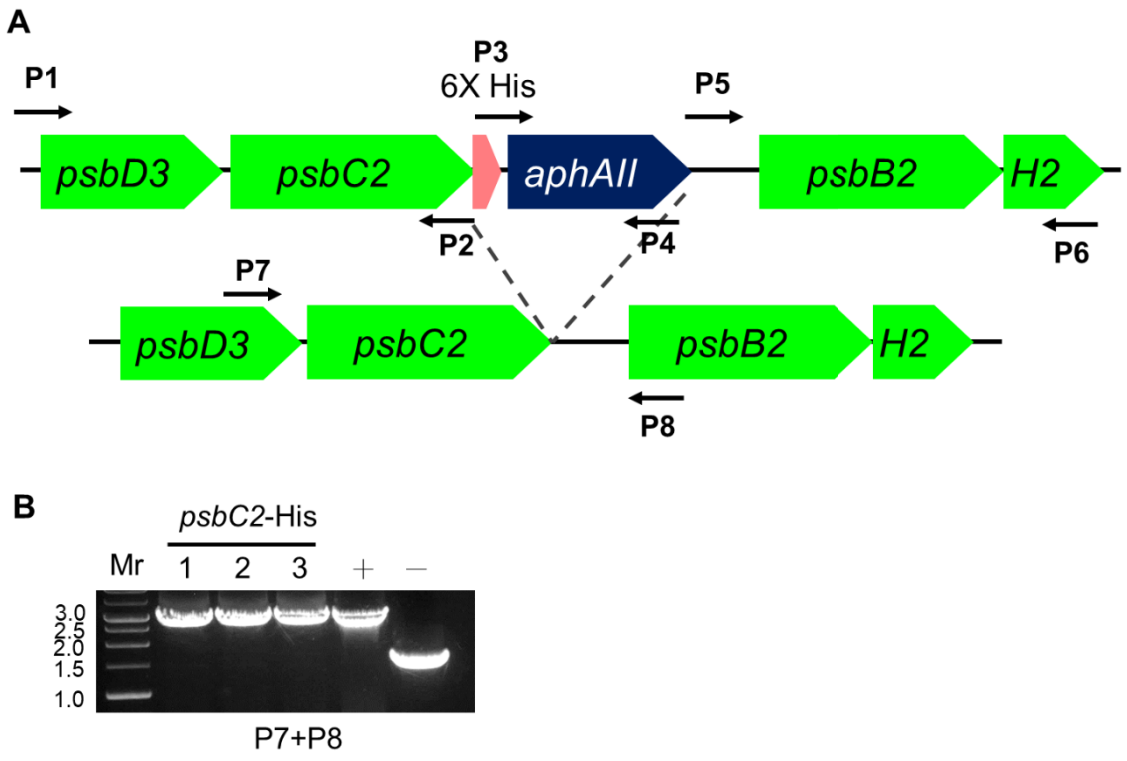


**Figure S1. Scheme showing a construct to express [His]$_6$-tagged *psbC2* in *Synechococcus* 7335.**

(**A**) Scheme showing the PCR-based strategy to generate a construction for replacement of the *psbC2* gene with a [His]$_6$-tagged *psbC2* in *Synechococcus* 7335. Sequences of primers are listed in **Table S1**. A kanamycin resistance cassette (blue, *aphAII)* was inserted downstream from [His]$_6$-tagged *psbC2* to facilitate selection. See Materials and Methods for more details. (**B**) Agarose gel electrophoresis of PCR amplicons produced by colony PCR of three selected transconjugants (lanes 1 to 3) to confirm successful insertion of [His]$_6$-tagged *psbC2* and the kanamycin resistance cassette. Lane Mr contains a DNA size ladder (sizes shown in kb to left), and + and — refer to lanes containing PCR amplicons using DNA templates for the positive control (conjugative plasmid) and negative control (WT genome). As shown, Km-resistant colonies showed the introduction of the [His]$_6$-tagged *psbC2* gene.

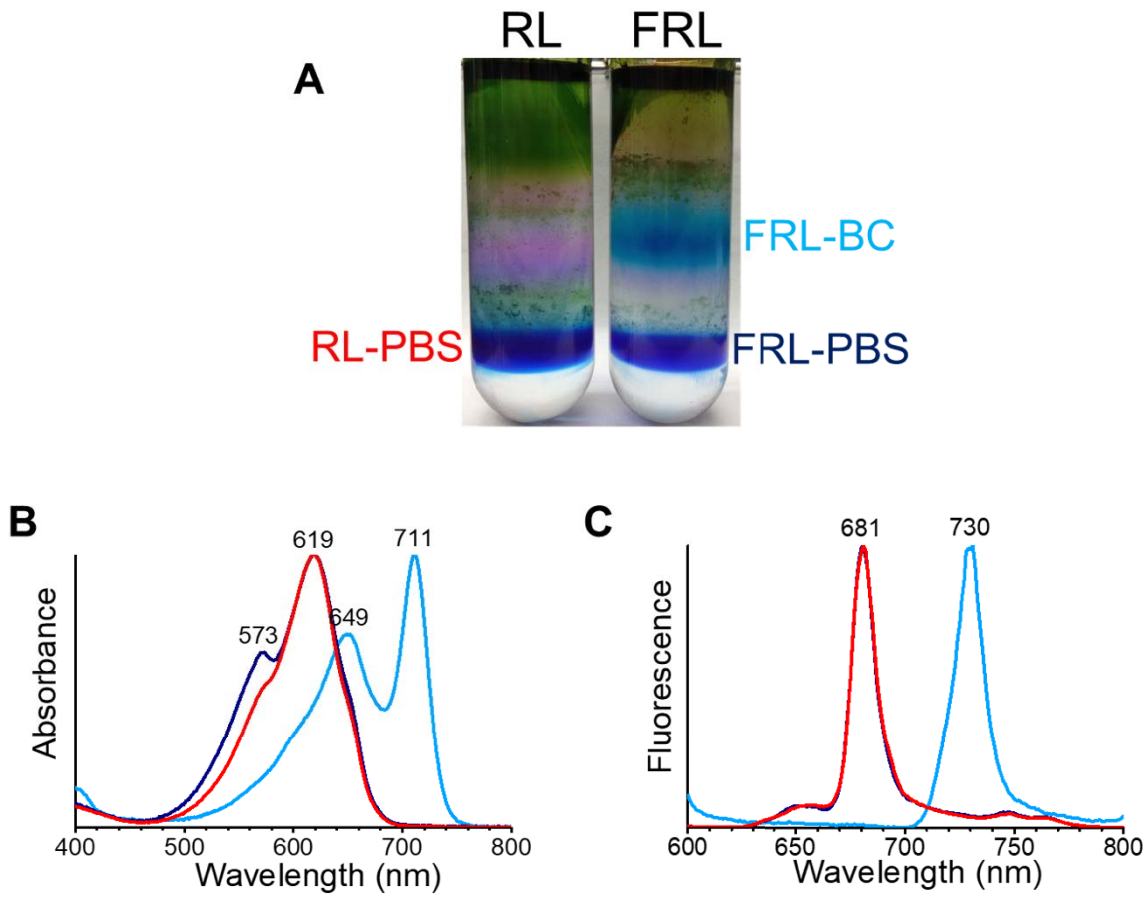


**Figure S2. Sucrose gradient centrifugation for isolation of PBS and FRL-BC from *Synechococcus* 7335.**

(**A**) Sucrose gradient centrifugation showing the separation of RL-PBS, FRL-BC, and FRL-PBS. (**B**) The steady-state absorption spectra of indicated samples. (**C**) The 77-K steady-state fluorescence emission spectra of indicated samples. RL-PBS, FRL-BC, and FRL-PBS are depicted in red, cyan, and blue, respectively. Note that the three indicated fractions are completely free of cross-contamination.

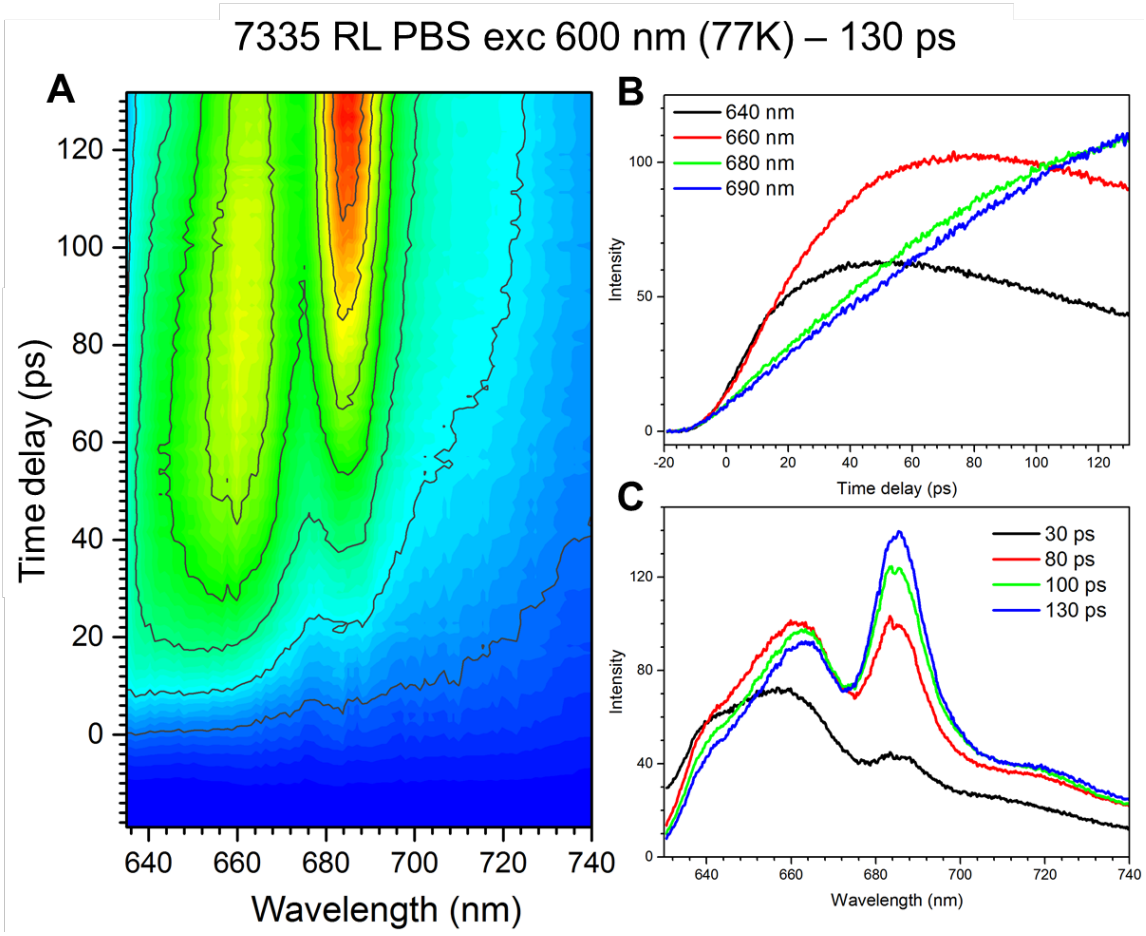


**Figure S3 Time-resolved fluorescence emission of RL-PBS excited at 600 nm (preferentially excites PBP, mostly PC but also AP) at 77 K in time range of 0 to 130 ps.**

(**A**) 3D-pseudocolor representation of the TRF results. The color in the 3D-pseudocolor diagram corresponds to the intensity of fluorescence emission. The gradient of intensity changes from lowest levels in blue shades to the highest levels in red shades. (**B**) Representative kinetic traces at the indicated wavelengths. (**C**) Examples of fluorescence emission spectra taken at the indicated delay times with respect to excitation at time 0.

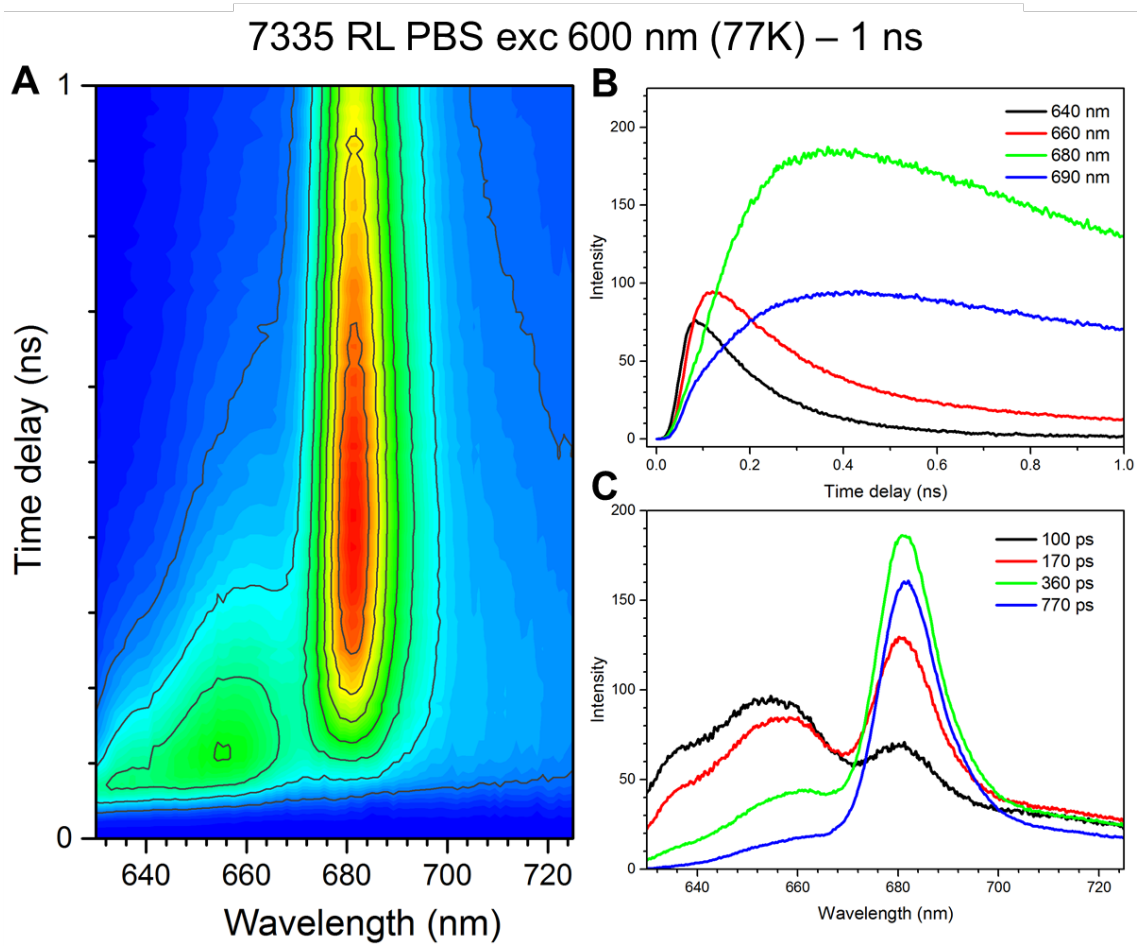


**Figure S4 Time-resolved fluorescence emission of RL-PBS excited at 600 nm (preferentially excites PBP, mostly PC but also AP) at 77 K in the time range from 0 to 1 ns.**

(**A**) 3D-pseudocolor representation of TRF results. The color in the 3D-pseudocolor diagram corresponds to the intensity of fluorescence emission. The gradient of intensity changes from lowest levels in blue shades to the highest levels in red shades. (**B**) Representative kinetic traces at the indicated wavelengths. (**C**) Examples of fluorescence emission spectra taken at the indicated delay times with respect to excitation at time 0.

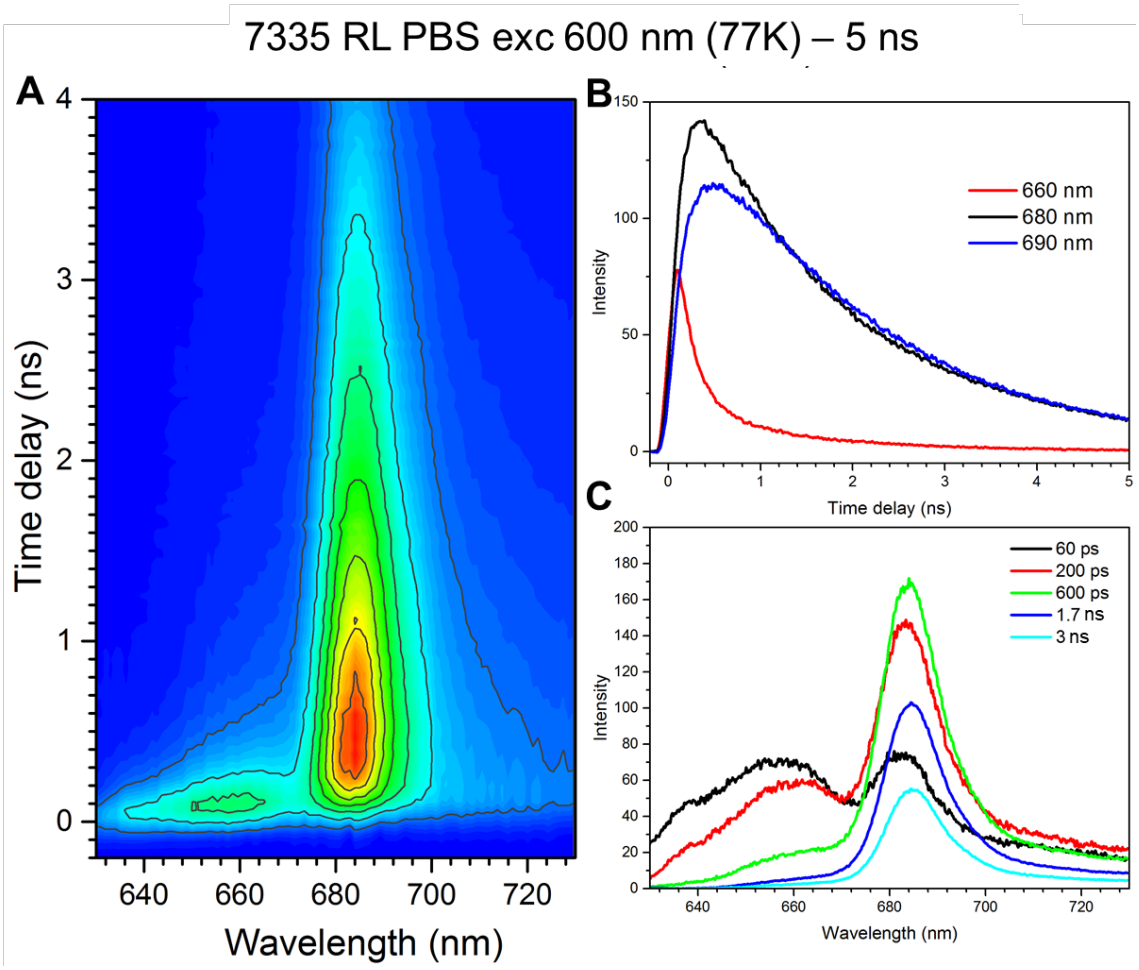


**Figure S5 Time-resolved fluorescence emission of RL-PBS excited at 600 nm (preferentially excites PBP, mostly PC but also AP) at 77 K in the time range from 0 to 4 or 5 ns.**

(**A**) 3D-pseudocolor representation of TRF results from 0 to 4 ns. The color in the 3D-pseudocolor diagram corresponds to the intensity of fluorescence emission. The gradient of intensity changes from lowest levels in blue shades to the highest levels in red shades. (**B**) Representative kinetic traces from time 0 to 5 ns at the indicated wavelengths. (**C**) Examples of fluorescence emission spectra taken at indicated delay times with respect to excitation at time 0.

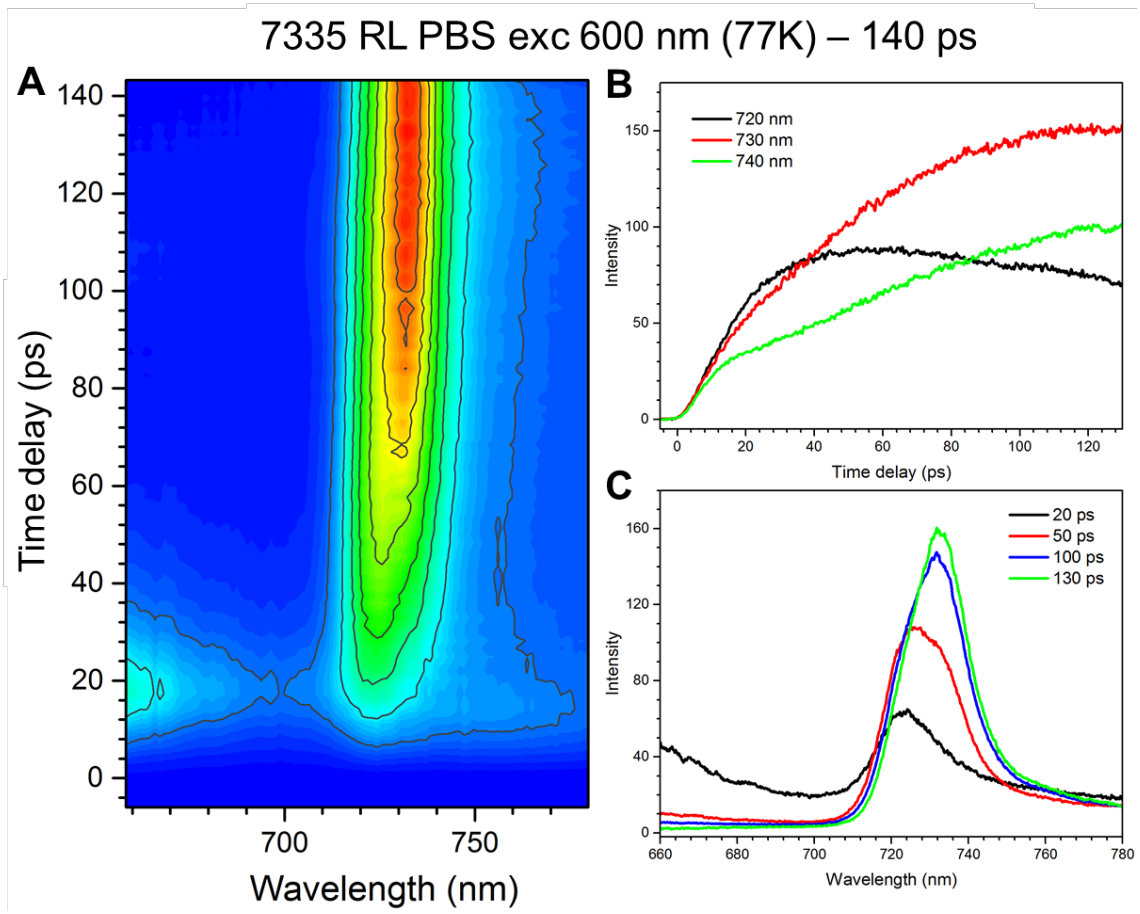


**Figure S6 Time-resolved fluorescence emission of FRL-BC excited at 600 nm (preferentially excites PBP, mostly FRL-AP) at 77 K in the time range from 0 to 140 ps**

(**A**) 3D-pseudocolor representation of TRF results from 0 to 140 ps. The gradient of intensity changes from lowest levels in blue shades to the highest levels in red shades. (**B**) Representative kinetic traces from time 0 to 130 ps at the indicated wavelengths. (**C**) Examples of fluorescence emission spectra taken at the indicated delay times with respect to excitation at time 0.

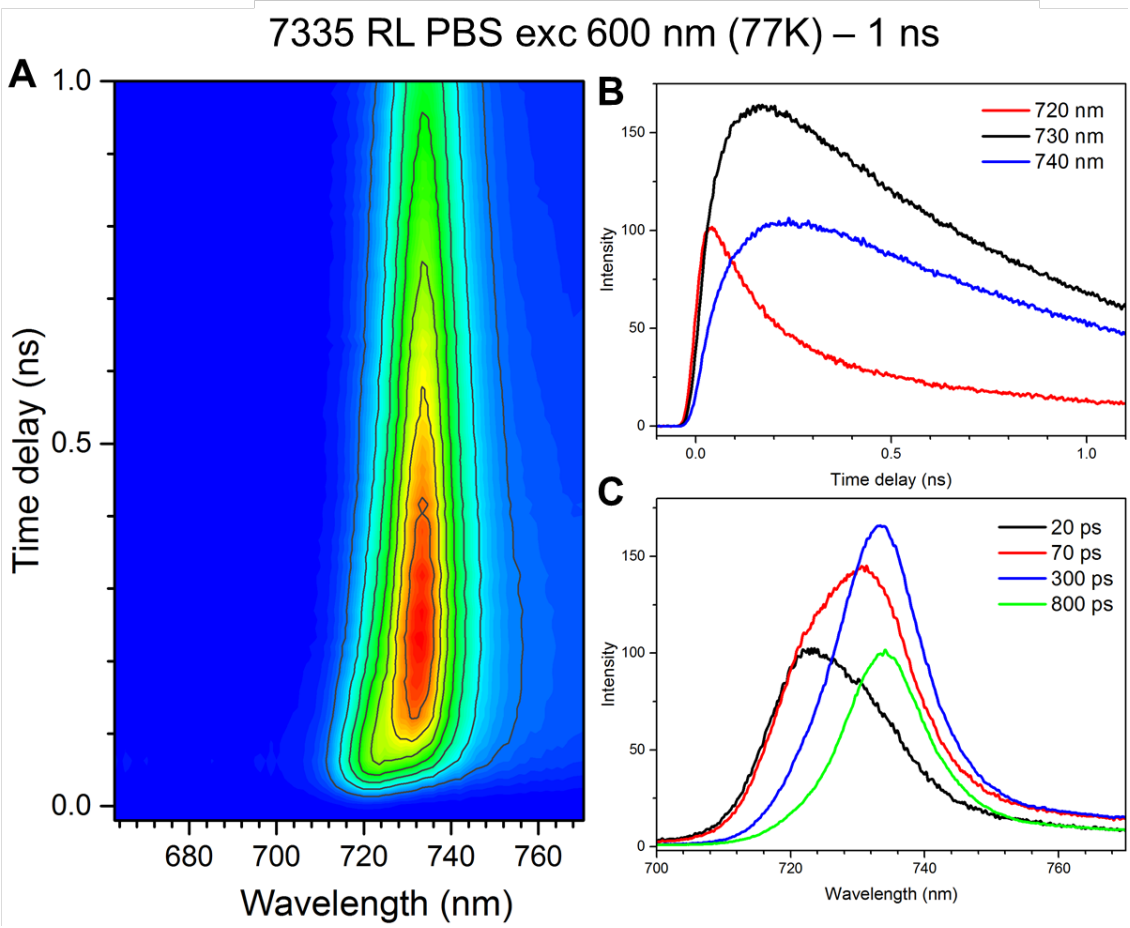


**Figure S7 Time-resolved fluorescence emission of FRL-BC excited at 600 nm (preferentially excites PBP, mostly FRL-AP) at 77 K in the time range from 0 to 1 ns**

(**A**) 3D-pseudocolor representation of TRF results from 0 to 1 ns. The color in the 3D-pseudocolor diagram corresponds to the intensity of fluorescence emission. The gradient of intensity changes from lowest levels in blue shades to the highest levels in red shades. (**B**) Representative kinetic traces from time 0 to 1 ns at the indicated wavelengths. (**C**) Examples of fluorescence emission spectra taken at the indicated delay times with respect to excitation at time 0.

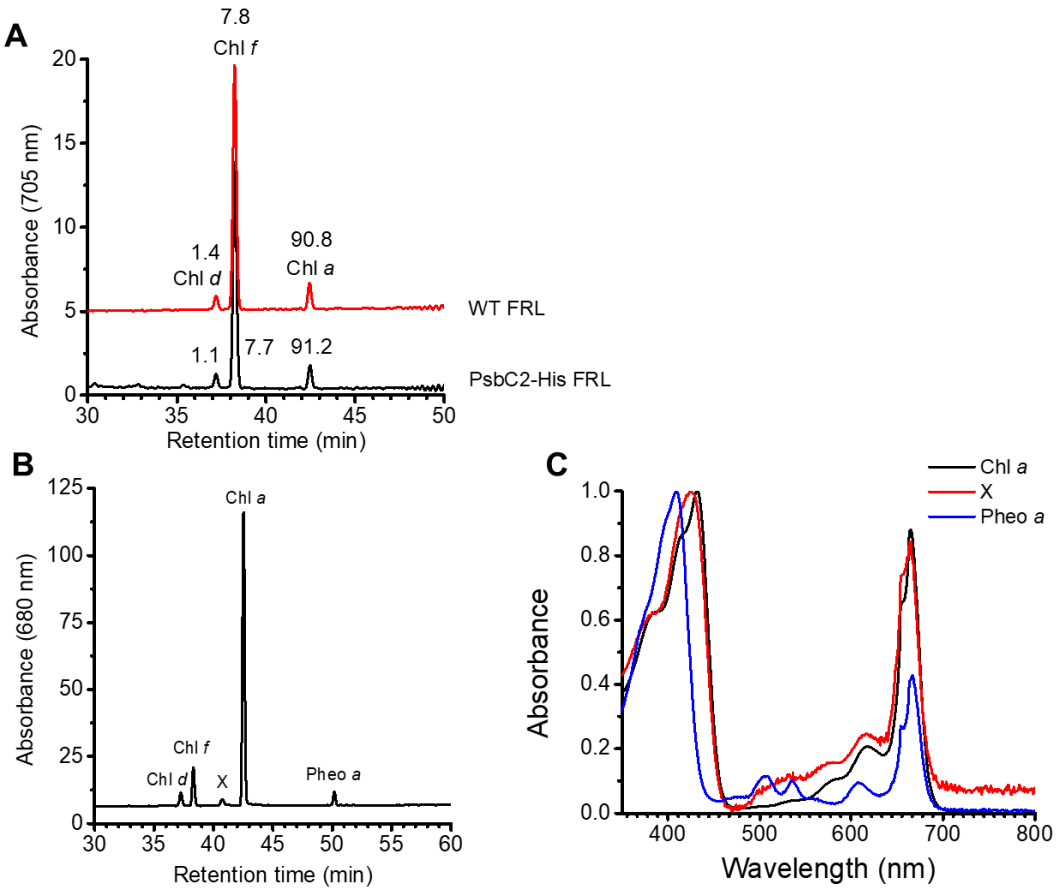


**Figure S8 Reversed-phase HPLC elution profile of pigments extracted from FRL-PSII and absorption spectra of selected pigments.**

(**A**) Separation of pigments from thylakoid membranes isolated from *Synechococcus* 7335 wild type in FRL (WT FRL) and from the strain producing a $[His]_6$-tagged variant of PsbC2 in FRL (PsbC2-His FRL). The numbers indicate the percentage of each Chl in total Chls. (**B**) Separation of pigments from purified FRL-PSII shows the presence of Chl *d*, Chl *f*, Chl *a*, pheophytin *a* (Pheo *a*) and pigment X. The absorbances at 680 nm approximately represent the ratios for Chl *d*: Chl *f*: Chl *a*. (**C**) Absorption spectra of Chl *a*, Pheo *a*, and X, showing that pigment X has an absorption spectrum similar to that of Chl *a*. Note that the small shoulders at ~650 nm in the absorption spectra are artifacts caused by a defective diode in the spectrophotometer.

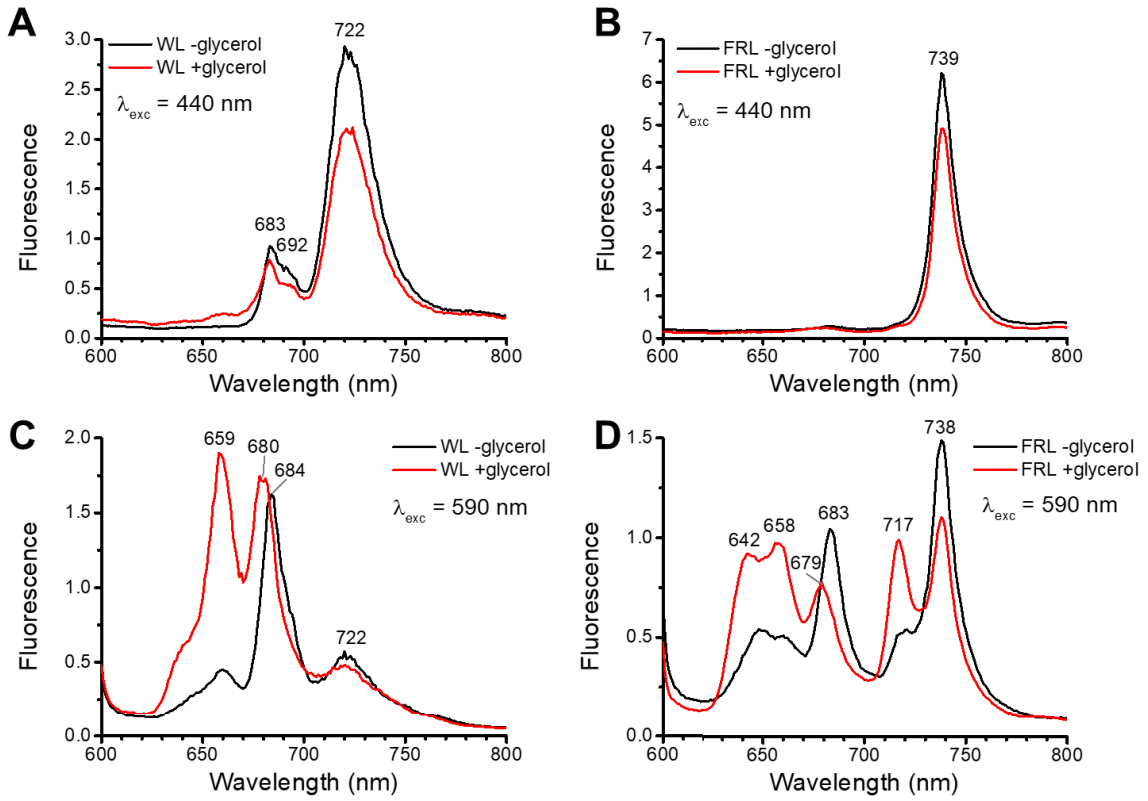


**Figure S9 Steady-state fluorescence emission spectra at 77 K of *Synechococcus* 7335 cells grown in WL and FRL.**

This measurement was used to test the effect of glycerol on the integrity of PBS/PBP and the energy transfer from PBP/PBS to PSII in intact cells. Fully acclimated *Synechococcus* 7335 cells grown in WL and FRL were harvested by centrifugation. The cell pellets from 1 ml of $OD_{750\ nm}$ = 0.5 of cells were resuspended in 1 ml of 50 mM Tris-HCl, pH 8.0, with or without 60 % glycerol and were incubated at room temperature for 5 min. The resulting samples were quickly frozen in liquid nitrogen for measurement of 77K fluorescence spectra. Cells in acclimated to WL were excited at 440 nm (**A**) and at 590 nm (**C**) to excite Chls and PBPs preferentially, respectively. Cells acclimated to FRL were excited at 440 nm (**B**) or at 590 nm (**D**) to excite Chls and PBPs preferentially, respectively. The results show clearly that the addition of glycerol to the cells has a very large disruption effect on energy transfer involving PBPs.

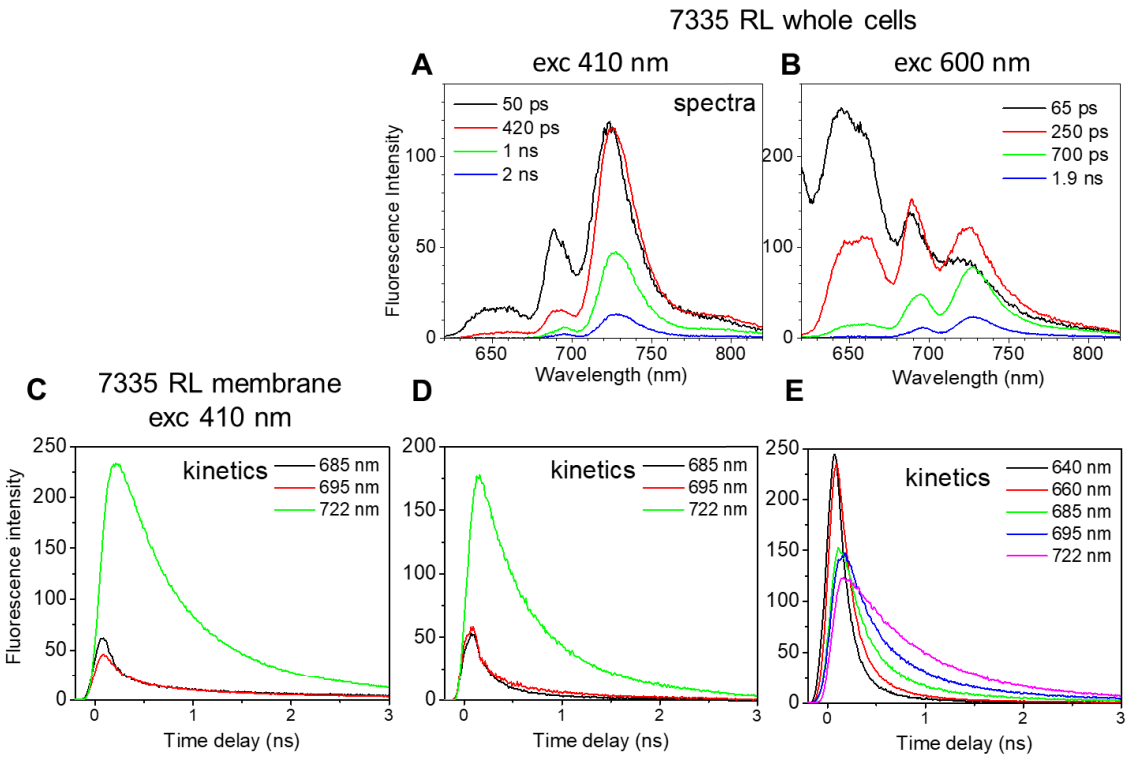


**Figure S10 Examples of time-resolved spectra and emission kinetics at selected wavelengths for thylakoid membranes and whole cells of RL-acclimated *Synechococcus* 7335.**

Whole cells grown in RL were excited at (**A**) 410 nm (preferentially excites Chl *a*) and (**B**) 600 nm (preferentially excited PBPs, mostly PC) at 77 K. (**A, B**). Examples of TRF spectra taken at the indicated delay times with respect to excitation at time 0 for excitation at 410 nm (**A**) or 600 nm (**B**). (**C-E**) Representative kinetic traces from time 0 to 3 ns at the indicated wavelengths after excitation at time zero for thylakoid membrane at 410 nm (**C**) and for whole cells at 410 nm (**D**) or 600 nm (**E**).

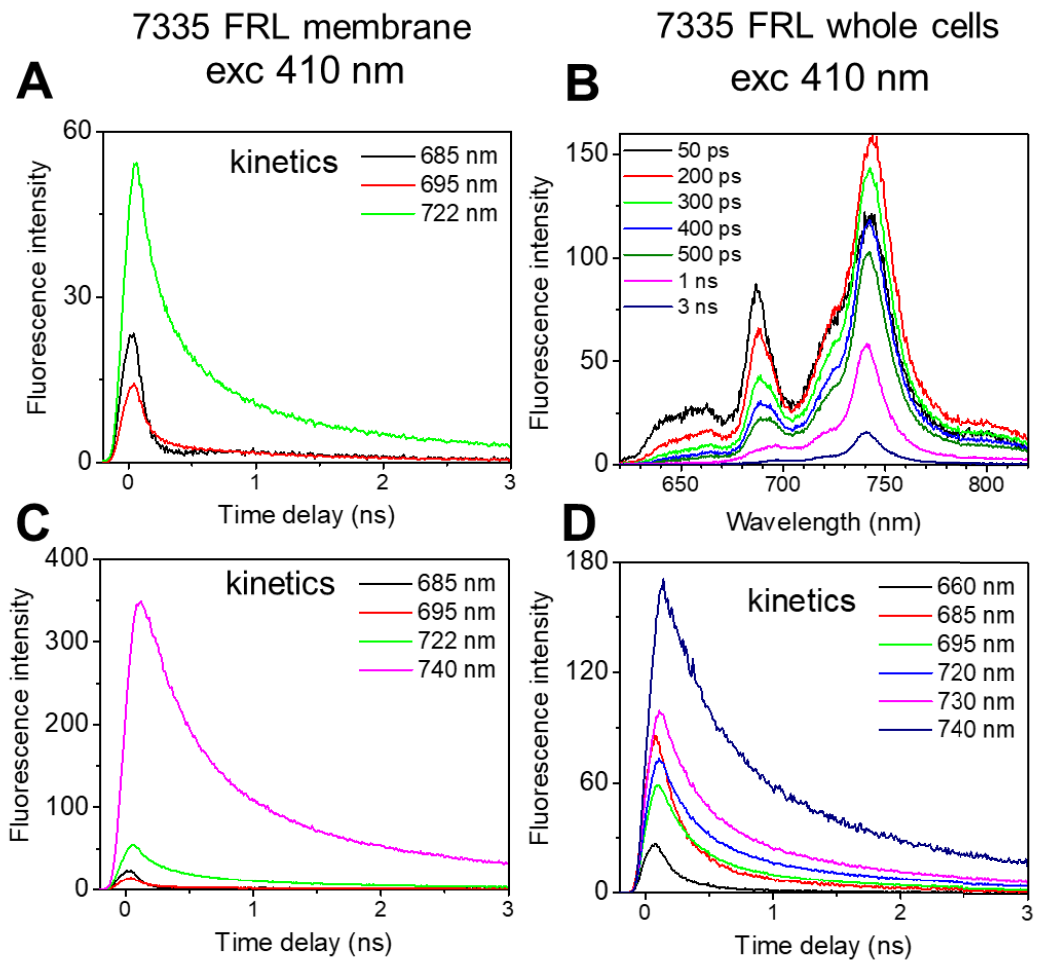


**Figure S11 Examples of fluorescence emission spectra and emission kinetics for thylakoid membranes and whole cells of *Synechococcus* 7335 grown in FRL after excitation at 410 nm at 77 K.**

Representative kinetic traces from time 0 to 3 ns at the indicated wavelengths for thylakoid membranes (**A** and **C**) and whole cells (**D**). Kinetics traces in panel **A** represent an enlarged version of three selected traces from panel **C**. (**B**) Examples of fluorescence emission spectra at the indicated delay times with respect to excitation at time 0.

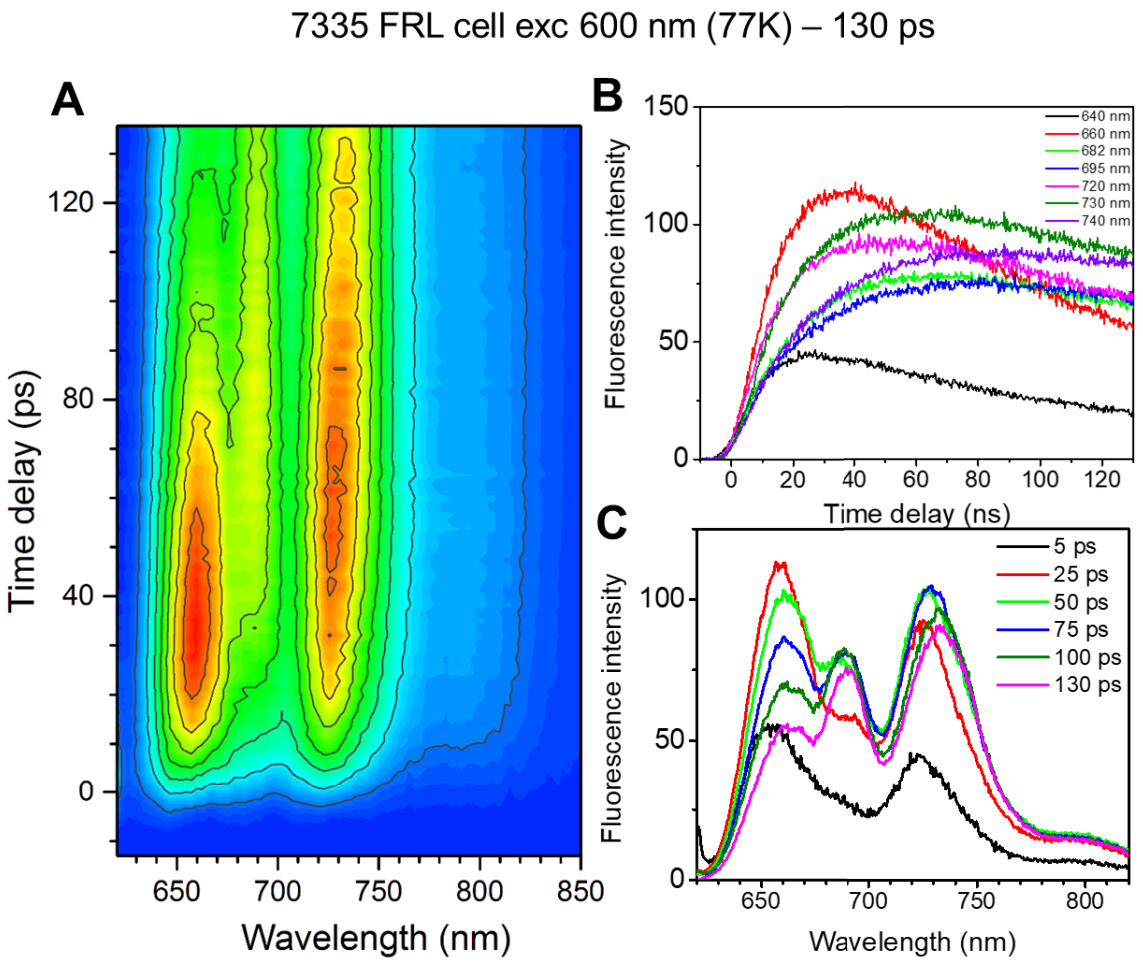


**Figure S12 Time-resolved fluorescence spectra of FRL-acclimated whole cells of *Synechococcus* 7335 excited at 600 nm (preferentially excites PBP) in the time range from 0 to 130 ps at 77 K.**

(**A**) 3D-pseudocolor representation of TRF results from 0 to 130 ps. The gradient of intensity changes from lowest levels in blue shades to the highest levels in red shades. (**B**) Representative kinetic traces from time 0 to 130 ps at the indicated wavelengths. (**C**) Examples of fluorescence emission spectra taken at the indicated delay times with respect to excitation at time 0.

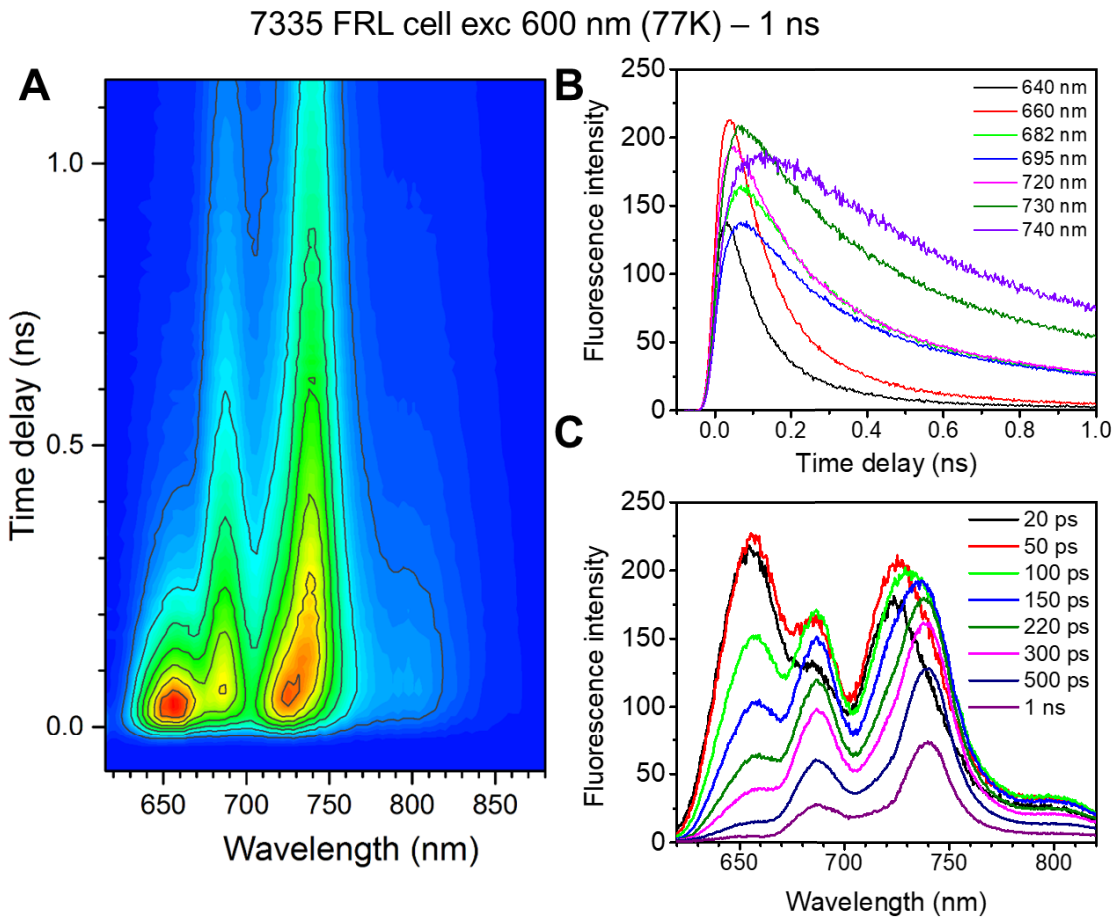


**Figure S13 Time-resolved fluorescence spectra of FRL-acclimated whole cells of *Synechococcus* 7335 excited at 600 nm (preferentially excites PBP) in the time range from 0 to 1 ns at 77 K.**

(**A**) 3D-pseudocolor representation of TRF results from 0 to 1 ns. The gradient of intensity changes from lowest levels in blue shades to the highest levels in red shades. (**B**) Representative kinetic traces from time 0 to 1 ns at the indicated wavelengths. (**C**) Examples of fluorescence emission spectra taken at the indicated delay times with respect to excitation at time 0.

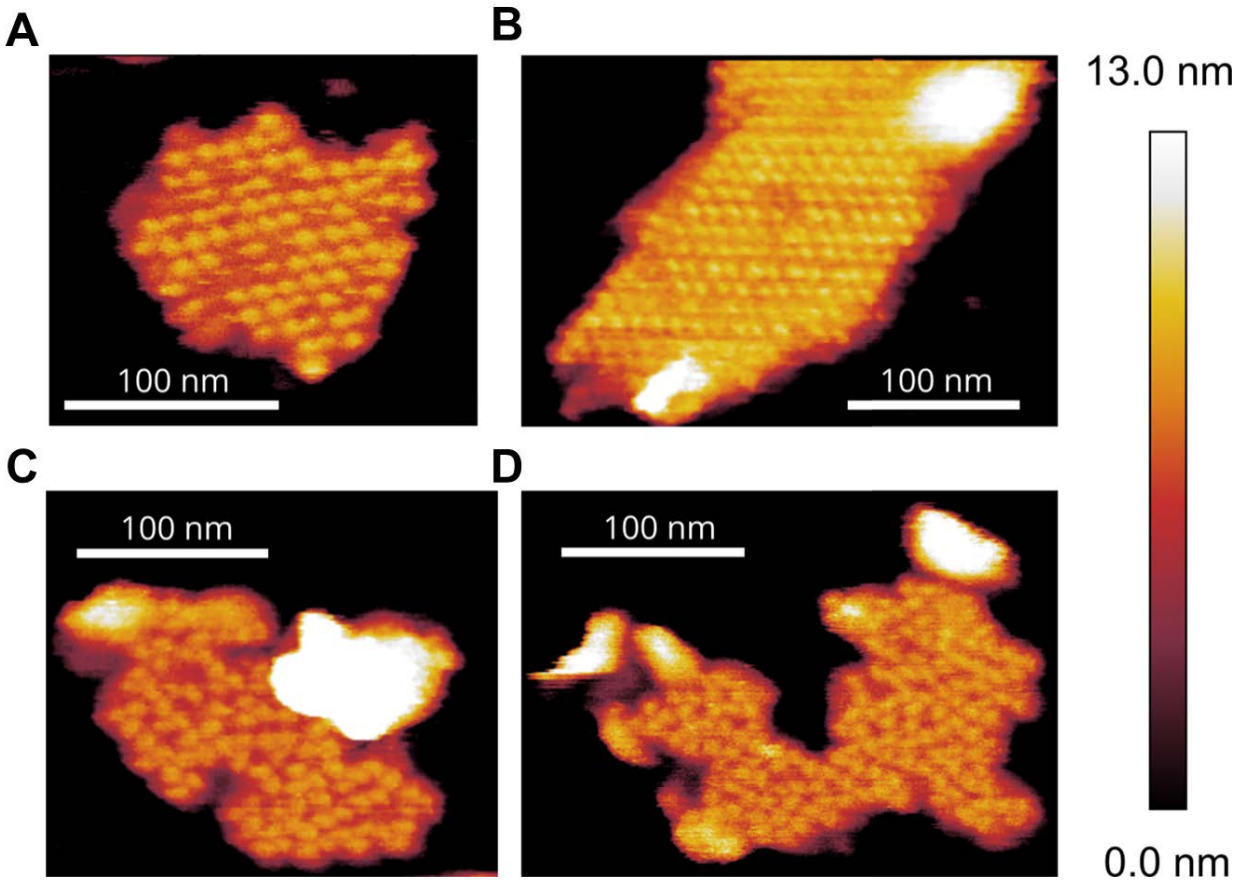


**Fig. S14. Additional AFM topographs of dimeric and trimeric PSI complexes in thylakoid membranes isolated from *Synechococcus* 7335 cells grown in RL**.

(**A**) PSI dimers, (B) PSI dimers, (C) "disorganized" PSI trimers and PSI dimers, and (D) disorganized PSI trimers.

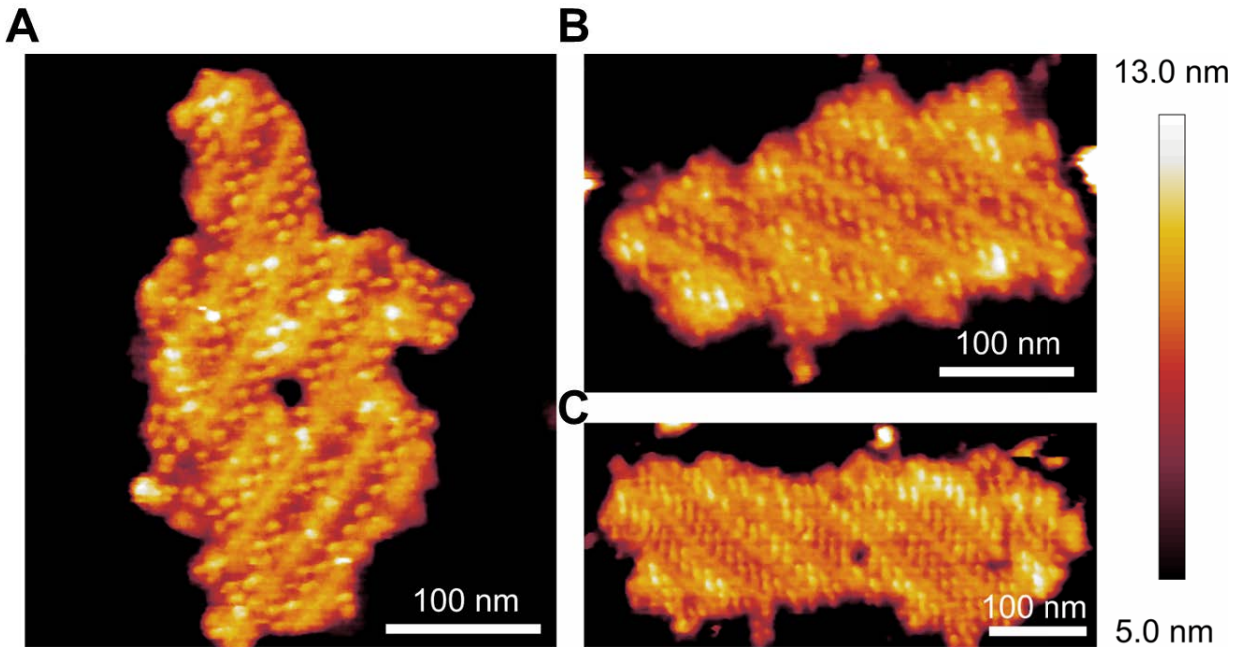


**Fig. S15. Additional AFM topographs showing alternating rows of monomeric (and/or dimeric) PSI and dimeric PSII complexes in thylakoid membranes isolated from *Synechococcus* 7335 cells grown in RL.**